IS-T-540

HIGH TEMPERATURE OXIDATION OF GADOLINIUM AND DYSPROSIUM UNDER CONTROLLED OXYGEN PARTIAL PRESSURE

M. S. Thesis Submitted to Iowa State University,
August, 1972

D. B. Basler

Ames Laboratory, USAEC
Iowa State University
Ames, Iowa 50010

Date of Manuscript: August, 1972

PREPARED FOR THE U. S. ATOMIC ENERGY COMMISSION
DIVISION OF RESEARCH UNDER CONTRACT NO. W-7405-eng-82

DISCLAIMER

Available from: National Technical Information Service
Department A
Springfield, VA. 22151

Price: Microfiche $0.95

High temperature oxidation of gadolinium and dysprosium under controlled oxygen partial pressures

by

David Bruce Basler

A Thesis Submitted to the
Graduate Faculty in Partial Fulfillment of
The Requirements for the Degree of
MASTER OF SCIENCE

Major: Ceramic Engineering

Approved:

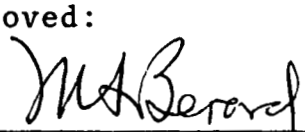

In Charge of Major Work

For the Major Department

For the Graduate College

Iowa State University
Ames, Iowa

1972

TABLE OF CONTENTS

High temperature oxidation of gadolinium and dysprosium under controlled oxygen partial pressures

David Bruce Basler

ABSTRACT

The oxidation of gadolinium and dysprosium was studied under controlled oxygen partial pressures in the temperature range 727-1327°C. The oxygen partial pressure range was $10^{-0.3}$ to $10^{-14.5}$ atm. Weight gain as a function of time was measured through the use of a thermobalance.

From the plots of rational scaling rate constant versus ln P_{O_2} it may be inferred that Gd_2O_3 exhibits p-type semiconductivity at oxygen pressures above $10^{-9.4}$ atm. in the temperature range 727-1177°C and that Dy_2O_3 exhibits p-type semiconductivity at oxygen pressures above $10^{-11.3}$ atm. in the temperature range 727-1327°C.

Utilizing the Wagner parabolic oxidation theory in the semiconducting range, self-diffusion coefficients of oxygen in Gd_2O_3 and Dy_2O_3 were found. The results are described by the relations

$$D = 1.149 \times 10^{-7} \exp\left(\frac{-40,269}{RT}\right) \text{ cm.}^2/\text{sec.}$$

for Gd_2O_3 (727-1177°C), and

$$D = 2.831 \times 10^{-8} \exp\left(\frac{-21,393}{RT}\right) \text{ cm.}^2/\text{sec.}$$

for Dy_2O_3 (727-1327°C).

INTRODUCTION

The lanthanide series elements are those which encompass atomic numbers 57 through 71. These particular elements are commonly called the rare earth elements, so appropriately named since they are relatively rare and all are metals found in nature as constituents of various minerals. Characteristic of these elements is that in increasing atomic number, electrons are added to the inner, well-shielded 4f shell rather than the outer 5d shell. A result of this is the lanthanide contraction; as atomic number increases, size decreases. Yttrium, atomic number 39, has a size comparable to the holmium-erbium region. For this reason and similarities in electron configuration, yttrium is included as a rare earth metal.

Gadolinium and dysprosium, the two metals of interest in this study, are members of this group of elements. They are atomic number 64 and 66, respectively. Gadolinium has an outer electron configuration of $4f^7 5d^1 6s^2$. The outer electron configuration of dysprosium is $4f^{10} 5d^0 6s^2$ (1). These two metals are quite similar in properties which can be seen in Table 1. In the ionic state, gadolinium has an outer electron configuration of $4f^7 5s^2 5p^6$, and dysprosium has $4f^9 5s^2 5p^6$ (1). The only valence of these metals is +3.

These metals have many industrial applications, but they have a great affinity for oxygen (ΔG°_{298} is approximately -400 kcal/mole for oxide formation) and, thus, no attainable

Table 1. Properties of gadolinium and dysprosium (2)

Property	Gadolinium	Dysprosium
Molecular weight	157.25	162.50
Melting point, °C	1312	1407
Density, g/cc	7.886	8.559
Boiling point, °C	3000	2600
Specific heat, cal/mole-°C (25°C)	8.80	6.73
Thermal conductivity, cal/cm^2-sec-°C/cm (28°C)	0.021	0.024
Thermal expansion, x10^6/°C	8.6 (25-950°C)	8.6
Crystal structure	HCP[a] BCC[b]	HCP
Transformation temperature, °C	1264 (3)	---
a_o, angstroms	HCP = 3.6360 BCC = 4.06	3.5903
Thermal neutron cross section, barns/atom	46,000±2000	1,100±150
Stable oxidation state	+3	+3
Young's modulus, x10^{-11} dynes/cm^2	5.62	6.31
Shear modulus, x10^{-11} dynes/cm^2	2.23	2.54
Curie temperature, °K	290	85
Resistivity, x10^6 ohm-cm (25°C)	140.5	91

[a]Hexagonal close packed.

[b]Body centered cubic.

environment can be realized in which these metals will not oxidize. Therefore, a practical limitation of these metals in use is that the oxidation not exceed an acceptable rate.

The only oxidation studies performed to date on these metals have been done in either dry air, moist air, or pure oxygen (4-23). A study done in controlled oxygen partial pressures will represent more realistic service conditions for these metals. The data obtained will allow prediction of oxidation during use.

The oxidation products are the sesquioxides of gadolinium and dysprosium. These ceramic materials lend themselves to use as refractory materials since they have high melting points. Also, due to the high thermal neutron cross section of the metals, the oxides have found use in control rods and shielding material in nuclear reactors. Some of the important properties of the oxides of gadolinium and dysprosium are given in Table 2.

The purpose of this research is the study of mass and charge transport during the high temperature oxidation of gadolinium and dysprosium under controlled oxygen partial pressures. Knowledge of oxidation rate constants as a function of temperature and oxygen partial pressure will allow prediction of the oxidation rates of these metals over a wide range of environments. Secondly, determination of diffusion coefficients of oxygen in the oxides as a function of temperature

Table 2. Properties of Gd_2O_3 and Dy_2O_3 (2)

Property	Gd_2O_3	Dy_2O_3
Molecular weight (all forms)	362.50	373.0
Color	White	White
Thermal expansion, $x10^{-6}/°C$	8.2 (100-1000°C)	7.7 (20-1300°C)
Crystal structure	Cubic Monoclinic Hexagonal[a]	Cubic Monoclinic[a] Hexagonal[a]
a_o, angstroms	Cubic = 10.19	Cubic = 10.63
Transition temperature, °C	Cubic to monoclinic = 1280 Monoclinic to hexagonal = 2125[a]	Cubic to monoclinic = 1850[a] Monoclinic to hexagonal = 2200[a]
Melting point, °C	2350	2340
Density, g/cc	7.407	7.81

[a]Foex and Traverse (24).

and oxygen partial pressure can aid in understanding sintering behavior and changes in stoichiometry of the oxides. Finally, analysis of the oxygen partial pressure dependence of the ionic and electronic conductivities will aid in explaining the exact mechanisms by which diffusion and electronic conduction can occur in the oxide.

RARE EARTH METAL OXIDATION

Starting with Loriers' study of cerium and lanthanum oxidation in 1949 (4), there have been several studies on the oxidation characteristics of the rare earth metals (4-23). These studies have been done in either dry air, moist air, or pure oxygen. These oxidation studies have labeled the oxidation behavior according to one of the four different rate laws: linear, parabolic, cubic, or logarithmic. The rate laws are of the form $w^n = kt$ which relate weight of oxide formed to time and k is the rate constant. Linear is when n = 1, parabolic is when n = 2, and cubic when n = 3. The logarithmic rate law is of the form $w = k \log(at+b)$ where a and b are constants. To date, the study of rare earth metal oxidation as a function of both oxygen partial pressure and temperature has not been done.

One of the most comprehensive rare earth metal oxidation studies was made by Greene and Hodge (5). The oxidation behavior was determined on all of the rare earths except promethium. Yttrium was included for study because of its similarity to the lanthanide elements. The oxidation was done in dry and moist air from 100-800°C. The results indicated that gadolinium, dysprosium, samarium, neodymium, and lutetium exhibited parabolic oxidation over the entire temperature range. Cerium and terbium oxidized paralinearly (initially parabolic followed by linear behavior) then finally oxidized

catastrophically at 300 and 400°C, respectively. Lanthanum, praseodymium, and europium also oxidized parabolically, but there were no data available above 400°C for these metals. Linear oxidation behavior was shown by holmium, erbium, thulium, and ytterbium. In addition, erbium oxidized catastrophically at 700°C. Yttrium showed very complex behavior. It first oxidized linearly up to 500°C. At 600°C, it initially oxidized linearly, then demonstrated a parabolic rate law. At 700°C, yttrium oxidized only in a parabolic manner, and at 800°C it followed a cubic law. All oxides formed were the sesquioxides except for terbium, cerium, praseodymium, europium, and samarium which showed additional oxide forms. Moist air increased oxidation rates and the oxidation behavior of cerium, praseodymium, europium, and terbium transformed from parabolic to linear kinetics. This transition in kinetics was a result of moisture promoting the formation of second oxide phases. For example, in moist air europium tended to form $Eu(OH)_2$ (hydrated $EuO \cdot H_2O$) instead of Eu_2O_3 and oxidized linearly. In dry air Eu_2O_3 was formed and europium oxidized parabolically.

Phillips (6) studied the oxidation behavior of cerium, praseodymium, neodymium, samarium, gadolinium, terbium, and holmium in an atmosphere of 55% relative humidity air in the temperature range 600-1200°C. The results showed linear oxidation behavior and the formation only of the sesquioxides for all metals studied. These results did not reveal additional oxide forms for cerium, praseodymium, samarium, and terbium as did the work of Greene and Hodge (5). The oxidation kine-

tics observed agreed with those of Green and Hodge except for gadolinium and neodymium.

Lee and Greene (7) examined the oxidation behavior of all the rare earths, including yttrium, except promethium and lutetium. The oxidation was done in dry air at 25, 100, and 200°C, in water-saturated air at 40°C, and in air at equilibrium with 30% hydrogen peroxide at 40°C. It was determined that lanthanum and cerium oxidized linearly and that praseodymium oxidized parabolically. The kinetics were not elucidated for the other metals studied. Lanthanum, cerium, and europium rapidly oxidized in room temperature air. All the other rare earths were not appreciably attacked by dry air at temperatures up to 200°C. Moisture again increased the oxidation rates.

Love (8) studied the oxidation of the rare earths, including yttrium, except promethium, europium, thulium, and lutetium in dry and moist air. The temperature range employed was 35-600°C. The results were not analyzed to determine oxidation kinetics, but several observations were made. First, the lighter elements, lanthanum, cerium, praseodymium, and neodymium had the most rapid oxidation rates. Samarium exhibited a very low rate of oxidation. At the highest temperatures, terbium oxidized much more readily than the other heavy rare earths. Overall, yttrium had a very low oxidation rate being faster only than samarium. Greene and Hodge (5) interpreted the kinetics of Love's study and gave the following summary: (a) lanthanum, neodymium, gadolinium, and terbium had parabolic behavior; (b) praseodymium and dysprosium oxidized linearly; (c) samarium oxidation was logarithmic; (d) holmium

and erbium oxidation was parabolic between 200-400°C and linear at 600°C and (e) no interpretation on the kinetics of cerium, ytterbium, and yttrium.

Vorres (9) and Vorres and Eyring (10) studied the oxidation behavior of lanthanum, cerium, praseodymium, neodymium, gadolinium, ytterbium, and samarium in oxygen between room temperature and 1200°C. All oxidized in a parabolic manner except cerium. Cerium oxidation was parabolic up to 187°C and linear thereafter. It was generally concluded that oxygen diffusion through the oxide layer was the oxidation mechanism on all of the metals with the possible exception of samarium. Additional oxide forms for cerium and praseodymium were observed, but such was not the case for samarium and ytterbium.

Edmondson et al. (11) examined the oxidation behavior of holmium, dysprosium, neodymium, praseodymium, thulium, yttrium, lutetium, and erbium in dry oxygen. Their results did not label oxidation behavior according to one of the rate laws, but, generally, the rate-controlling step was the diffusion of oxygen through a protective oxide coating. In later stages of reactions, particularly at low temperatures, there were deviations from parabolic kinetics.

Although Greene and Hodge (5) found parabolic oxidation for lanthanum, Loriers (4), Phillips (12) and Pethe et al. (13) found different oxidation behavior. Loriers (4) showed that, in dry air, lanthanum oxidized until a constant weight increase of 0.45 mg./cm.^{2} was obtained after 25 minutes at

300°C. Phillips (12) found linear behavior between 600 and 850°C with a discontinuous jump to a constant value of 32 ± 1.0 mg./cm.^{2}. This jump occurred at different times with each temperature as it was a function of the temperature. In both cases, once the constant weight gain was obtained no further weight gain was observed. This behavior was not observed by Pethe et al. (13). Their results indicated cubic oxidation behavior for lanthanum in the temperature range 500-700°C and at an oxygen pressure of 100 torr. The time of oxidation was much longer in this study than the previous two and a constant weight gain was not observed.

The oxidation of cerium, specifically, was studied by Loriers (4,14) in dry air and Cubicciotti (15) in oxygen. Cerium oxidized parabolically at temperatures below 125°C. Between 125 and 200°C, it initially had parabolic behavior followed by linear oxidation. At temperatures above 200°C, cerium oxidized in a linear manner.

Glushkova et al. (16) studied the oxidation behavior of neodymium in dry oxygen and air. It was found that at temperatures below 250°C the behavior was linear, but above this temperature neodymium showed parabolic behavior. The assessment of the oxidation mechanism is somewhat complicated by the formation of both the cubic (C) and hexagonal (A) forms of Nd_2O_3. In air, the C form was produced starting at room temperature. At about 350°C, the A form began to appear. In dry oxygen, however, the oxidation was first evident at 250°C with

the formation of A type Nd_2O_3 and the rate of oxidation was less than that in dry air. The following two mechanisms of oxidation were given as most probable: (a) migration of anions via anionic vacancies and (b) migration of cations via cationic vacancies. When the cubic form of Nd_2O_3 was formed, mechanism (a) was considered most likely. An explanation was not given for the formation of the A-type oxide.

As previously described, Greene and Hodge (5) found the oxidation behavior of yttrium to be quite complex. Borchardt (17) provided a more detailed study of yttrium oxidation. This study involved air oxidation at 900 and 1400°C. It was found that oxygen is quite soluble in yttrium. It was proposed that oxidation of yttrium has initially two competing reactions: (a) the dissolution reaction the rate of which is determined by the diffusion of oxygen through the metal and (b) the scale formation reaction. Initially (a) is the most rapid. As saturation is approached, (b) becomes predominant and parabolic behavior is observed. Greene and Hodge (5) generally supported the Borchardt mechanism. However, it was felt that the actual mechanism may be more complex since Y_2O_3 was observed to undergo a change in the oxide microstructure between 500 and 600°C. Haefling et al. (18) measured yttrium oxidation in air between 500 and 1400°C. At temperatures up to 875°C, there was deviation from parabolic oxidation behavior in the early stages. After the first few hours, there was

no additional weight gain indicating that a protective oxide layer had formed. At temperatures above 900°C, the oxidation was very rapid resulting in complete oxidation of the metal. Carlson et al. (19) studied yttrium oxidation in air between 450 and 925°C. The oxidation behavior was quite complex and was catastrophic at 925°C.

D'Souza et al. (20) studied the oxidation of gadolinium in the temperature range of 500-700°C and at an oxygen pressure of 100 torr. Mixed linear and parabolic behavior was observed. This study, done in a pure oxygen atmosphere, found parabolic oxidation behavior at 500 and 550°C. At 600, 650, and 700°C the oxidation was initially linear then parabolic. D'Souza et al. concluded that the oxidation of gadolinium involved diffusion of oxygen ions by means of anion vacancies in the oxide layer.

Dysprosium oxidation was studied from 500-800°C at an oxygen pressure of 100 torr by Pethe et al. (21). It was found that dysprosium oxidized according to the parabolic law over the entire temperature range. The oxidation proceeded by diffusion of oxygen via anion vacancies in the oxide layer.

In summary, past oxidation studies of the rare earth metals, including yttrium, generally describe the oxidation behavior of gadolinium, dysprosium, samarium, neodymium, lutetium, and perhaps yttrium to exhibit high temperature parabolic oxidation. It is this author's belief that yttrium probably oxidizes in a complex manner and possibly will

oxidize catastrophically as 900-1000°C is approached. The remaining rare earth metals oxidize linearly or exhibit complex behavior due to multiple oxidation states.

THEORY

General Parabolic Theory

In addition to Wagner's treatise on the theory of parabolic oxidation (25) (see next section), there have been several pioneering developments, review articles, and books on metal oxidation theory which should be mentioned (26-34). The Pilling-Bedworth rule (26) offers a means of mathematically determining which type of rate law, parabolic or linear, any metal should follow during oxidation. This is done by comparing the volume of one mole of oxide to the volume of metal required to produce one mole of oxide. If the ratio is greater than one, the oxide formed is compact and continuous (i.e., parabolic oxidation). If the ratio is less than one, a porous oxide coating is formed and linear oxidation is the rule. The Pilling-Bedworth ratio is

$$\frac{W \rho_m}{w \rho_{ox}} = \text{volume ratio} \qquad (1)$$

where

W = molecular weight of oxide

w = formula weight of metal (in this study, twice the atomic weight of the metal is used since the rare earth oxide formed is of the type M_2O_3)

ρ_{ox} = density of oxide

ρ_m = density of metal

For gadolinium, the ratio is 1.227. The ratio is 1.258 for dysprosium. Therefore, according to the Pilling-Bedworth rule

these metals should oxidize parabolically. It should be noted that, although this is a valid test, it is not the only factor determining the type of oxidation.

Hoar and Price (27) derived an electrochemical interpretation of Wagner's parabolic oxidation theory. A compact oxide on the surface of a metal can be regarded as a current-producing cell with the metal/oxide interface as the anode and the attacking gas/oxide interface as the cathode. For the case of the oxide layer having constant specific conductivity across the thickness

$$\frac{d\eta}{dt} = \frac{E_o(t_1+t_2)t_3kA}{F\delta} \qquad (2)$$

where

$\frac{d\eta}{dt}$ = rate of film growth (equivalents of oxide/sec.)

E_o = EMF across the oxide layer (volts)

t_1, t_2, t_3 = mean transference numbers of cation, anion, and electrons respectively

k = measured specific conductivity $(\text{ohm-cm.})^{-1}$

A = area of oxide layer (cm.^2)

F = Faraday's constant (coulomb/equivalent)

δ = scale thickness (cm.)

Separating variables, setting $\delta = W\eta/A\rho$, and integrating Eq. 2 gives

$$\eta^2 = \frac{2E_o(t_1+t_2)t_3kA^2\rho_{ox}}{FW}(t) \qquad (3)$$

where

t = time (sec.)

ρ_{ox} = density of oxide (gm./cc.)

W = gram-equivalent weight of oxide (gm./equivalent)

When the conductivity of the film varies with the partial pressure of the attacking gas

$$\frac{d\eta}{dt} = \frac{(t_1+t_2)t_3k_1A}{F\delta} \cdot \frac{aRT}{zF}\left[(P^o_{O_2})^{1/a} - (P^i_{O_2})^{1/a}\right] \qquad (4)$$

where

k_1 = specific conductivity in $k = k_1 P_x^{1/a}$

a = negative constant when the oxide is n-type semiconductor and positive constant when the oxide is p-type semiconductor

R = universal gas constant

T = temperature (°K)

z = valence of oxygen

$P^o_{O_2}$ = gas partial pressure at gas/oxide interface

$P^i_{O_2}$ = gas partial pressure at metal/oxide interface (equilibrium dissociation pressure of M_2O_3)

Equation 4 was not integrated, but to do so would yield the familiar parabolic equation.

Miley (28) and Hamilton and Miley (29), using an electrochemical interpretation, derived the linear, parabolic, and logarithmic rate laws. Since this study is only concerned with parabolic oxidation, the linear and logarithmic laws of Miley will not be presented. The parabolic law is

$$\frac{d\delta}{dt} = \frac{E_o(t_1+t_2)t_3kW}{\rho_{ox}F\delta} \qquad (5)$$

where

$d\delta/dt$ = rate of film thickness growth

E_o = EMF across the oxide

t_1, t_2, t_3 = transference numbers of cation, anion, and electrons respectively

k = measured specific conductivity of oxide

W = gram-equivalent weight of the oxide

ρ_{ox} = density of the oxide

F = Faraday's constant

δ = film thickness

Separating variables and integrating Eq. 5 gives the familiar parabolic equation

$$\delta^2 = \frac{2E_o(t_1+t_2)t_3kJ}{Fd}(t) + C \qquad (6)$$

where

C = integration constant

There has been much published on the theory of metal oxidation. Grimley (30) and Seybolt (31) have, perhaps, provided the better review articles on the theory of metal oxidation. The theory of the rate laws is presented along with examples of past studies on several different metals. Kofstad (32), Hauffe (33), and Kubaschewski and Hopkins (34) have summarized the tremendous volume of literature on metal oxidation theory and oxidation studies in book form. The important facts on theory are presented along with the most significant findings on various metal oxidation studies.

Wagner Parabolic Oxidation Theory

In 1933, Wagner (25) formulated a theory of parabolic oxidation of metals. This type of oxidation is expected to occur when there is the formation of a thick, coherent, and protec-

tive oxide scale. In this theory, it is assumed that the rate-determining process is either volume diffusion of the reacting ions or transport of electrons across the growing scale. As diffusion through the scale is rate-determining, reactions at phase boundaries are considered to be rapid, and thermodynamic equilibrium is established between the oxide and the atmosphere at the oxide/atmosphere interface and between the metal and the oxide at the metal/oxide interface. As a result, concentration gradients are established within the oxide.

The driving force of the oxidation reaction is the free energy change associated with the formation of the oxide. In other words, the parabolic oxidation of a pure metal is an electrochemical process in which there is movement of ionic species through the scale to a reaction interface accompanied by simultaneous movement of electronic defects to preserve charge neutrality. The treatment of Wagner's analysis which follows is extended to allow partition into ionic and electronic contributions. This has been verified by Hauffe (35) and Heyne (36).

In the growing oxide scale there are a number of types of moving particles. These particles are electrons (or holes), oxygen ions, and metal ions. The electrons and metal ions move from the metal surface toward the oxide/atmosphere interface. Oxygen ions (and holes, if applicable) move from the oxide/oxygen interface toward the metal/oxide interface. The local flux of any specific kind of particle can be expressed as

$$J_i = c_i v_i \tag{7}$$

where

J_i = local flux of species i (equivalents/cm.^{2}-sec.)

c_i = local concentration of species i (equivalents/cm.^{3})

v_i = local velocity of species i (cm./sec.)

Also

$$v_i = b_i \Sigma F_n \tag{8}$$

where

b_i = mobility of species i (cm.^{2}-particle/joule-sec.)

F_n = individual virtual driving forces acting on a particle (Newton/part.)

Substitution of Eq. 8 into Eq. 7 leads to

$$J_i = c_i b_i \Sigma F_n \tag{9}$$

For the oxidation process, it can be assumed that gradients in chemical potential (μ_i) and electrical potential (ϕ) are the only important virtual driving forces. These two potentials can be combined into a single electrochemical potential (η_i) given by

$$\eta_i = \mu_i + Nz_i e\phi \tag{10}$$

where

N = Avogadro's number

z_i = valence of species i (including sign)

e = electronic charge

Thus, the total virtual driving force on the species can be taken as the negative of the gradient of the electrochemical potential in the x direction.

$$\Sigma F_n = \frac{-\partial \eta_i}{\partial x} = -\frac{d\mu_i}{dx} - Nz_i e \frac{d\phi}{dx} \qquad (11)$$

Substituting Eq. 11 into Eq. 9 and dividing by N to put potentials on a per particle basis

$$J_i = -c_i b_i \left[\frac{1}{N} \frac{d\mu_i}{dx} + z_i e \frac{d\phi}{dx} \right] \qquad (12)$$

where

$\frac{d\mu_i}{dx}$ = chemical potential gradient of species i (joules/mole-cm.)

$\frac{d\phi}{dx}$ = electrical potential gradient (volts/cm.)

The electrical potential gradient ($d\phi/dx$) is not an externally imposed gradient as is $d\mu_i/dx$. Instead, it would develop internally if the charged particle fluxes did not exactly cancel at every point in the oxide scale. For gadolinium and dysprosium the sesquioxides are the oxidation product, therefore $z_1 = +3$ (cation), $z_2 = -2$ (anion), and $|z_3| = 1$ (electrons or holes). Mobility is defined as

$$b_i = \frac{\sigma t_i}{Fe|z_i|c_i} \qquad (13)$$

where

σ = conductivity (1/ohm-cm.)

t_i = transference number of species i

F = Faraday's constant (96,500 coulombs/equivalent)

Substitution of Eq. 13 into Eq. 12

$$J_i = \frac{-\sigma t_i}{Fe|z_i|} \left[\frac{1}{N} \frac{d\mu_i}{dx} + z_i e \frac{d\phi}{dx} \right] \qquad (14)$$

The flux of the species can be pictured

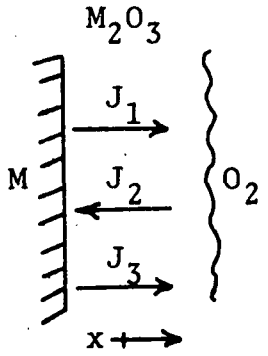

The flux equations for each species are

$$J_1 = \frac{-\sigma t_1}{Fe|z_1|}\left[\frac{1}{N}\frac{d\mu_1}{dx} + z_1 e\frac{d\phi}{dx}\right] \tag{15}$$

$$J_2 = \frac{-\sigma t_2}{Fe|z_2|}\left[\frac{1}{N}\frac{d\mu_2}{dx} - z_2 e\frac{d\phi}{dx}\right] \tag{16}$$

$$J_3 = \frac{-\sigma t_3}{Fe|z_3|}\left[\frac{1}{N}\frac{d\mu_3}{dx} - z_3 e\frac{d\phi}{dx}\right] \tag{17}$$

Since the units on J_i are equivalents/cm^2.-sec., the requirement that no positive or negative charges accumulate at any point in the scale is expressed by

$$J_1 = J_2 + J_3 \tag{18}$$

Combining Eqs. 15, 16, 17, and 18 and solving for $d\phi/dx$

$$\frac{d\phi}{dx} = -\frac{1}{N}\left[\frac{t_1}{|z_1|}\frac{d\mu_1}{dx} - \frac{t_2}{|z_2|}\frac{d\mu_2}{dx} - \frac{t_3}{|z_3|}\frac{d\mu_3}{dx}\right] \tag{19}$$

The following ionization reactions can be written

$$\text{cation} + |z_1| \text{ electrons} = \text{metal atom}$$

$$\text{anion} = \text{oxygen atom} + |z_2| \text{ electrons}$$

Using the above reactions as applied to free energy changes (conditions of equilibrium)

$$\mu_1 + |z_1|\mu_3 = \mu_m \tag{20}$$

$$\mu_2 = \mu_x + |z_2|\mu_3 \tag{21}$$

where

μ_m = chemical potential of metal atoms

μ_x = chemical potential of oxygen atoms

One form of the Gibbs-Duhem relationship is $N_m d\mu_m + N_x d\mu_x = 0$. Assuming that virtual stoichiometry is maintained in the oxide, $N_m/N_x = |z_2|/|z_1|$. Using the virtual stoichiometric assumption, the Gibbs-Duhem relationship and Eqs. 20 and 21 in Eqs. 15, 16, and 17 gives

$$J_1 = \frac{t_1 t_3 \sigma}{FNe}\left[-\frac{1}{|z_1|}\frac{d\mu_m}{dx}\right] \tag{22}$$

$$J_2 = \frac{t_2 t_3 \sigma}{FNe}\left[\frac{1}{|z_1|}\frac{d\mu_m}{dx}\right] \tag{23}$$

$$J_3 = \frac{(t_3+t_2) t_3 \sigma}{FNe}\left[-\frac{1}{|z_1|}\frac{d\mu_m}{dx}\right] \tag{24}$$

The total ionic charge flux is $J_{12} = J_1 + J_2 = |J_3|$. Then

$$J_{12} = |J_3| = \frac{(t_1+t_2) t_3 \sigma}{FNe\,|z_1|}\left|\frac{d\mu_m}{dx}\right| = \frac{(t_1+t_2) t_3 \sigma}{FNe\,|z_2|}\left|\frac{d\mu_x}{dx}\right| \tag{25}$$

Then,

$$J_{12}dx = \frac{(t_1+t_2) t_3 \sigma}{FNe\,|z_2|} d\mu_x \tag{26}$$

Integrating Eq. 26 over the scale thickness yields

$$J_{12}\delta \equiv K_r = \frac{1}{FNe} \int_{\mu_x^i}^{\mu_x^o} \frac{(t_1+t_2)t_3\sigma}{|z_2|} d\mu_x \qquad (27)$$

where

K_r = rational scaling rate constant (equivalents/cm.-sec.)

δ = scale thickness (cm.)

μ_x^o = chemical potential (joules/mole) at oxide/gas interface

μ_x^i = chemical potential (joules/mole) at metal/oxide interface

For metal oxidation by oxygen (x = atomic oxygen)

$$\mu_x = \mu_o = 1/2\mu_{O_2}$$

$$\mu_x = \mu_O^o + RT \ln P_O = 1/2\mu_{O_2}^o + 1/2RT \ln P_{O_2}$$

$$d\mu_x = \frac{RT}{2} d \ln P_{O_2}$$

$$|z_2| = 2$$

Using the above relationships and k (Boltzmann constant) = R/N in Eq. 27 gives

$$J_{12}\delta = K_r = \frac{kT}{4Fe} \int_{P_{O_2}^i}^{P_{O_2}^o} (t_1+t_2)t_3\sigma d \ln P_{O_2} \qquad (28)$$

where

$P_{O_2}^o$ = oxygen partial pressure at oxide/atmosphere interface (fixed experimentally)

$P_{O_2}^i$ = oxygen partial pressure at metal/oxide interface (fixed by free energy of formation of oxide)

Using the relationships between transference number and total conductivity ($\sigma_{ionic} = t_{ionic}\sigma_T$ and $\sigma_e = t_e\sigma_T$) plus t_1+t_2 =

t_{ionic} and $t_e = t_3$ (T = total, and e = electronic) in Eq. 28 gives

$$J_{12}\delta = K_r = \frac{kT}{4Fe} \int_{P^i_{O_2}}^{P^o_{O_2}} \frac{\sigma_{ionic}\sigma_e}{\sigma_T} \, d \ln P_{O_2} \qquad (29)$$

where

σ_{ionic} = partial ionic conductivity

σ_e = partial electronic conductivity

σ_T = total conductivity

Equation 29 shows that the slower moving species is rate-controlling.

When the oxide is behaving as a semiconductor ($t_e \cong 1$), Eq. 29 becomes

$$J_{12}\delta = K_r = \frac{kT}{4Fe} \int_{P^i_{O_2}}^{P^o_{O_2}} \sigma_{ionic} \, d \ln P_{O_2} \qquad (30)$$

and the movement of ionic species is seen to be rate-limiting. The Nernst-Einstein equation relating ionic conductivity and self-diffusion coefficients is

$$\frac{\sigma_i}{D_i} = \frac{c_i^* z_i^2 e^2}{kT}$$

where

c_i^* = concentration of ith species (ions/cm^3)

D_i = self-diffusion coefficient of species i (cm^2/sec.)

Substitution of this equation into Eq. 30 gives

$$K_r = \frac{e}{4F} \int_{p_{O_2}^i}^{P^o_{O_2}} (D_1 c_1^* z_1^2 + D_2 z_2^2 c_2^*) d \ln P_{O_2} \qquad (31)$$

Berard et al. (37) have shown that oxygen is the more mobile ionic species in the rare earth oxides. Equation 31 with $D_2 >> D_1$ becomes

$$K_r = \frac{e}{F} \int_{P^i_{O_2}}^{P^o_{O_2}} D_2 c_2^* d \ln P_{O_2} \tag{32}$$

where

c_2^* = concentration of oxygen in oxide (ions/cm.^{3})

When the oxide is an ionic conductor ($t_{ionic} \cong 1$), the movement of the electronic species is rate-controlling and Eq. 29 becomes

$$J_{12}\delta = K_r = \frac{kT}{4Fe} \int_{P^i_{O_2}}^{P^o_{O_2}} \sigma_e d \ln P_{O_2} \tag{33}$$

Wagner's theory presents a relationship between the parabolic rate constant and the rational scaling rate constant. The rate of increase in thickness of the oxide coating is inversely proportional to thickness. The proportionality constant is the parabolic rate constant.

$$\frac{d\delta}{dt} = \frac{K_p}{\delta} \tag{34}$$

where

K_p = parabolic rate constant

Solving Eq. 34

$$\frac{\delta^2}{t} = 2K_p \tag{35}$$

At any specific time

$$V = \delta A \tag{36}$$

where

A = area of sample ($cm.^2$)

V = volume of oxide coating ($cm.^3$)

$$v = \frac{M}{\rho} \tag{37}$$

v = equivalent volume of oxide ($cm.^3$)

M = equivalent weight of oxide (gm.)

ρ = density of oxide ($gm./cm.^3$)

$$n = \frac{V}{v} = \frac{\delta A}{v} \tag{38}$$

n = number of equivalents in oxide scale of thickness δ

Differentiating Eq. 38 with respect to time gives

$$\frac{dn}{dt} = \frac{A}{v} \frac{d\delta}{dt} \tag{39}$$

Flux, J_{12}, is defined as equivalents/$cm.^2$-sec. which is $(dn/dt)/A$ and (from Eq. 27) it is equal to K_r/δ. Substituting this relationship into Eq. 34 gives

$$K_r = \frac{1}{v} K_p \tag{40}$$

In this study, weight gain is measured as a function of time. Wagner has related this measurement to K_r in the following way: At any given time

$$\Delta W = \frac{nW_a}{|z_2|} \tag{41}$$

where

ΔW = weight gain of the original sample (mg.)

W_a = atomic weight of oxygen

Substituting Eq. 38 into Eq. 41 and solving for δ yields

$$\delta = \frac{\Delta W v z_2}{A W_a} \tag{42}$$

Using Eq. 42 in 35 gives

$$2K_p = \frac{\Delta W^2 v^2 |z_2|^2}{A^2 W_a^2 t} = \frac{1}{t}\left(\frac{\Delta W}{A}\right)^2 \left[\frac{|z_2| v}{W_a}\right]^2 \tag{43}$$

Defining the experimental quantity $K_s \equiv 1/t(\Delta W/A)^2$ and solving Eq. 43 gives

$$K_p = \frac{1}{2}\left[\frac{|z_2| v}{W_a}\right]^2 K_s \tag{44}$$

Combining Eq. 40 and Eq. 44 yields

$$K_r = \frac{1}{2} v \left[\frac{|z_2|}{W_a}\right]^2 K_s \tag{45}$$

Thus, weight gain as a function of time can be related to the rational scaling rate constant. Wagner's parabolic oxidation theory provides a means of using the rational scaling rate constants so obtained to calculate oxygen diffusion coefficients when the oxide behaves as a semiconductor and to obtain electronic conductivity information when the oxide is behaving as an ionic conductor.

EXPERIMENTAL PROCEDURE

Metal Selection

The discussion on previous rare earth metal oxidation studies has shown that gadolinium, dysprosium, neodymium, samarium, lutetium, and, perhaps, yttrium exhibit parabolic oxidation behavior. Only two of these metals, gadolinium and dysprosium, were chosen for analysis in this study. Since this study has engineering value and all of these metals are in use, it should be noted why these two particular metals were selected.

Samarium was not a suitable metal to study since it forms a multilayer oxide scale (5). Both oxidation states of +2 and +3 are stable forms for samarium (2), and Wagner's oxidation theory assumes the same oxide layer throughout.

Another factor to consider in determining which metals to study is the polymorphism of the oxides. It was desired to avoid polymorphic transformations in the experimental range. This behavior in rare earth oxides has been extensively studied (24,38-44). From Table 2, gadolinium oxide has both cubic and monoclinic forms. Foex and Traverse (24) have shown this transformation to be near 1300°C and irreversible. Roth and Schneider (38) and Warshaw and Roy (39) also found the cubic to monoclinic transformation to be near this temperature. Since the melting point of gadolinium is 1312°C, the highest temperature for experimentation on gadolinium will be somewhat

below the oxide transformation temperature. Dysprosium oxide transforms from cubic to monoclinic near 1850°C (24) which is well above the experimental temperature range. Neodymium oxide has an irreversible transformation from cubic to hexagonal about 600°C (24,38,39). Others (16,40,41) have reported this transformation to take place between 800 and 1100°C. Due to the possibility of this irreversible, reconstructive transformation being in the experimental temperature range neodymium was not chosen for this study.

Yttrium, although it has been shown by some investigators to exhibit parabolic oxidation (17), was not selected for study. Greene and Hodge (5) showed quite complex oxidation behavior for yttrium and Haefling et al. (18) and Carlson et al. (19) reported that yttrium oxidizes catastrophically around 900°C. Since yttrium has not clearly been shown to oxidize parabolically, it was not studied.

Lutetium, due to its high cost, has not been in practical use and so was not chosen for this study.

Materials

The main experimental procedure involved the controlled oxidation of small metal specimens under fixed conditions of temperature and oxygen partial pressure. The metals used, gadolinium and dysprosium, were obtained from the Ames Laboratory in distilled, arc melted button form. They were submitted to the metal fabrication shop for rolling to 10 mil thickness

and annealing. Analysis of the metals as received is shown in Table 3. Hydrogen, oxygen, and nitrogen were measured by vacuum fusion techniques. Carbon was measured by combustion-chromatographic techniques, fluorine by the distillation and the determination of fluosilicic acid, and iron by solution-spectrophotometric techniques. The rare earth and other impurities in dysprosium were found by emission spectroscopy and wet methods, as spark source mass spectrometry was not available. All analyses for rare earth and other impurities in the gadolinium were made by spark source mass spectrometry.

The 10 mil metal sheets were cut into rectangles, 6.35 mm. by 3.175 mm. A hole, 12 mil diameter, was drilled in the upper center portion of each specimen. Immediately prior to oxidation the metal specimens were polished under mineral oil using 600 grit silicon carbide paper, cleaned in trichloroethylene, and rinsed in methyl alcohol. This was done to remove any grease or other dirt from handling plus any oxide coating that may have been present on the metal surface.

Apparatus

A Cahn RG Electrobalance was used to measure weight gain of the specimens during oxidation. This balance allows for the continuous measurement of weight change in milligrams. This weight gain was input to one channel of a dual-channel chart recorder (Honeywell, Electronik 194). The second channel gave a continuous recording of the temperature.

Table 3. Analyses of metals in ppm. by weight

Element	Dysprosium	Gadolinium
H	N.D.[a]	1.2
O	255	50
N	102	16
C	50	9
F	894	118
Fe	≤70	0.8
Y	≤10	2.5
La	N.M.[b]	21.2
Ce	N.M.	0.8
Pr	N.M.	2.0
Nd	N.M.	24.8
Sm	N.M.	<0.3
Eu	N.M.	<0.2
Gd	≤200	10^6
Tb	≤500	≤0.3
Dy	10^6	<0.4
Ho	≤100	0.3
Er	≤50	<0.3
Tm	N.M.	<0.2
Yb	N.M.	≤11
Lu	N.M.	2.2
Others	≤380	≤54.5

[a]Not detected.

[b]Not measured, as spark source mass spectrometry not available.

The specimens were suspended from the balance by a 10 inch sapphire rod and a 2 inch quartz rod, each with a 10 mil diameter, hooked together. Figure 1 shows the balance and furnace arrangement. These rods were rigid and would not react under the oxidizing conditions. The furnace was of molybdenum-wound alumina muffle construction. The casing was water-cooled steel. In the space between the casing and the muffle tube, helium was circulated to prevent the molybdenum from oxidizing.

Temperature was measured by the use of a Pt-Pt,10% Rh thermocouple. Through careful measurement, the thermocouple was so placed in the furnace (from the bottom) to be in the hot zone virtually next to the suspended specimen. Temperature stability during a run was maintained by keeping the furnace voltage and current constant. Figure 2 shows the equipment arrangement.

To obtain the desired oxygen partial pressure, mixtures of Ar-O_2, CO_2-CO, and specially ordered mixtures of these gases were used. The special mixtures were 1,000 ppm. O_2-balance Ar, and 100 ppm. CO-balance CO_2. These mixtures were necessary in order to obtain the entire P_{O_2} range at most temperatures. Through the use of a cartesian diver, the total furnace pressure was maintained at 0.5 atmospheres.

Using Ar-O_2, the P_{O_2} is determined by

$$P_{O_2} = \frac{\dot{n}_{O_2}}{\dot{n}_t} \; P_t \qquad (46)$$

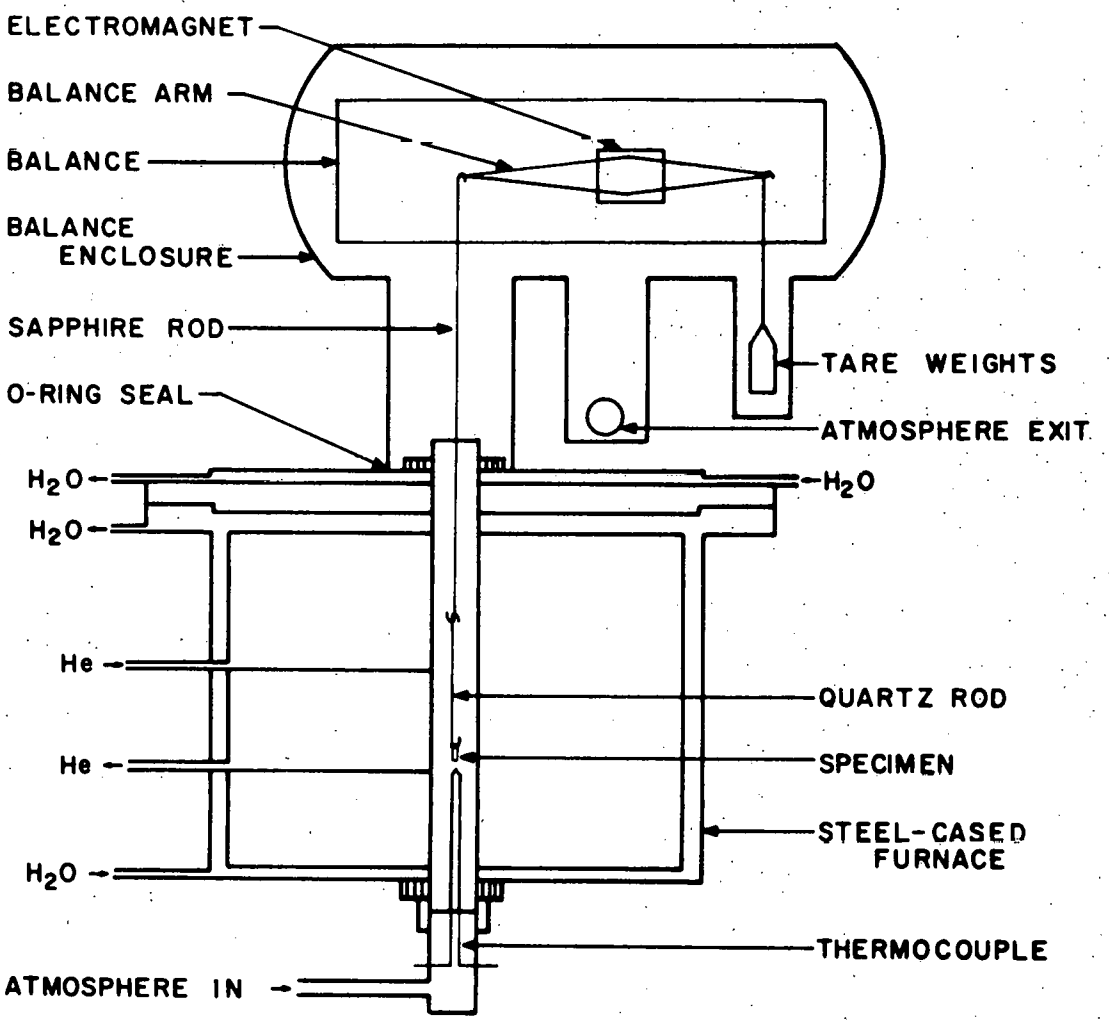

Figure 1. Furnace, balance, and specimen arrangement

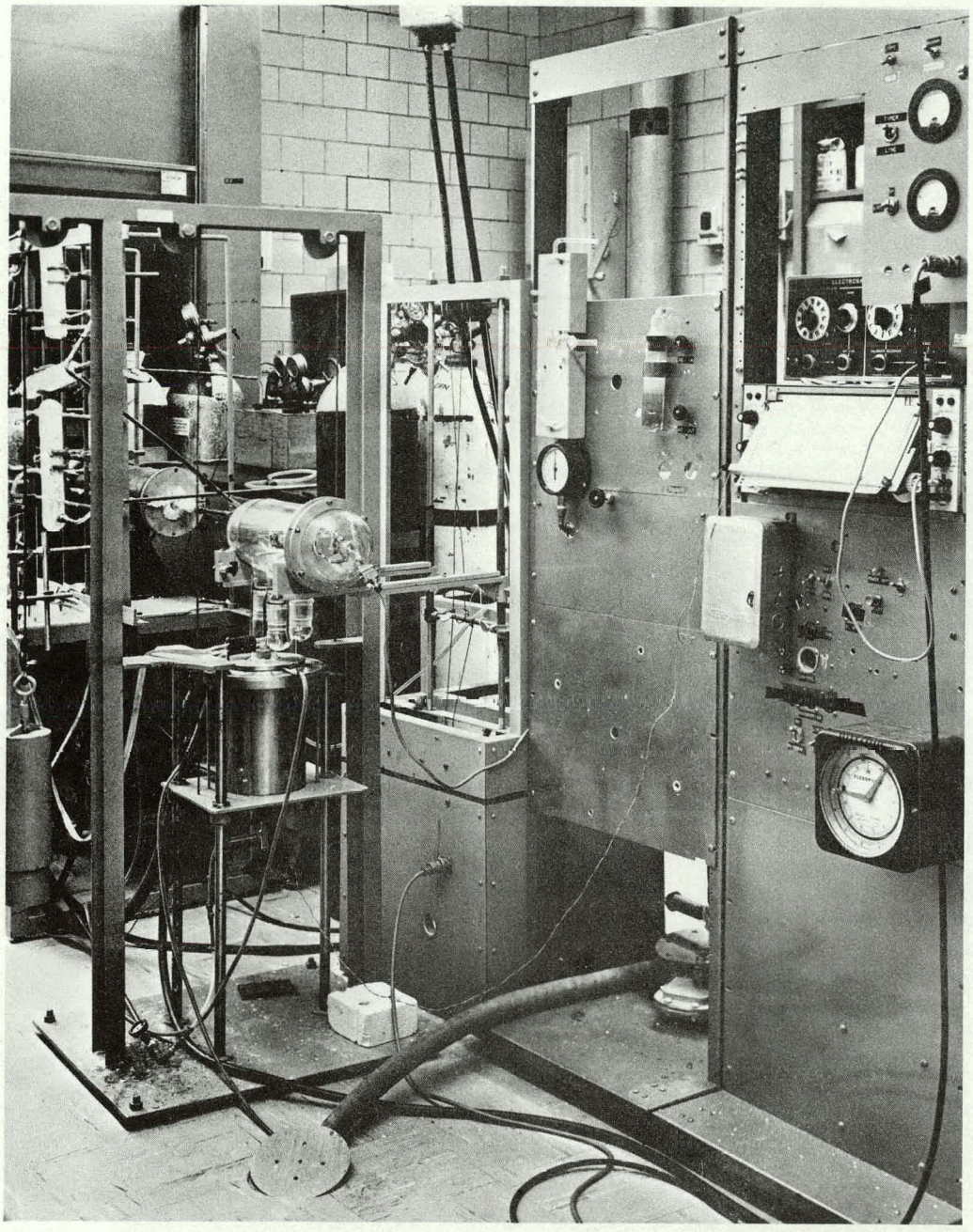

Figure 2. The electrobalance, gas train, and associated equipment

where

$\dot{n}_{O_2}$ = flow rate of oxygen (ml./min.)

$\dot{n}_t$ = total flow rate $(\dot{n}_{O_2}+\dot{n}_{Ar})$(ml./min.)

P_t = total pressure inside furnace (atm.)

Using CO_2-CO, the P_{O_2} is determined by

$$\log P_{O_2} = 2\log \frac{\dot{n}_{CO_2}}{\dot{n}_{CO}} + \frac{2\Delta G_T^\circ}{2.303RT} \qquad (47)$$

where

$\dot{n}_{CO_2}$ = flow rate of carbon dioxide (ml./min.)

$\dot{n}_{CO}$ = flow rate of carbon monoxide (ml./min.)

ΔG_T^o = standard free energy of the reaction for oxidation of a mole of CO to CO_2 at temperature T (kcal/mole)

R = universal gas constant (kcal/mole-°K)

T = temperature (°K)

Equation 47 was derived from the reaction $1/2\ O_2 + CO \rightleftarrows CO_2$ using thermodynamic relationships and flowrates. ΔG_T^o was calculated for the given reaction using data from Wicks and Block (45).

To purify, dry, and blend the gases, a gas train was constructed using anhydrous magnesium perchlorate (anhydrone) to remove water, sodium hydrate asbestos absorbent (ascarite) to remove CO_2, and heated (600°C) copper turnings to remove O_2 by the oxidation of Cu to CuO. Although the gases were mixed upon leaving the flowmeters, an additional chamber filled with

glass beads was used to insure complete mixing. A diagram of the gas train is contained in Figure 3.

The flow rates of the individual gases were regulated by two rotameter-type flowmeters (Matheson Gas Products, Model No. 610). An additional flowmeter was used to regulate the flow rate of the mixed gases into the furnace. These flowmeters had calibration curves, supplied by the manufacturer, for the gases that were used. However, a check was made of the calibration using a method as explained by Levy (46). This method involves measuring the time for a soap bubble being pushed by the flowing gas to sweep out a calibrated volume (graduated cylinder). The check performed found the calibration curves to be accurate.

Procedure

Immediately after the specimens were polished and cleaned, they were attached to the quartz fiber. The quartz fiber was then hooked to the long sapphire rod already suspended from the left side of the balance beam (see Figure 1). The weight of the two rods and the specimen were then tared out and the balance was turned on. The furnace was then raised up over the sample to join with the balance enclosure. The vacuum pump was turned on to seal the furnace to the balance enclosure and to remove the atmosphere present in the system. The gases were turned on, flow rate established, and then allowed to flow for fifteen to forty-five minutes prior to heating of the furnace. This time was allowed to insure the desired atmosphere was

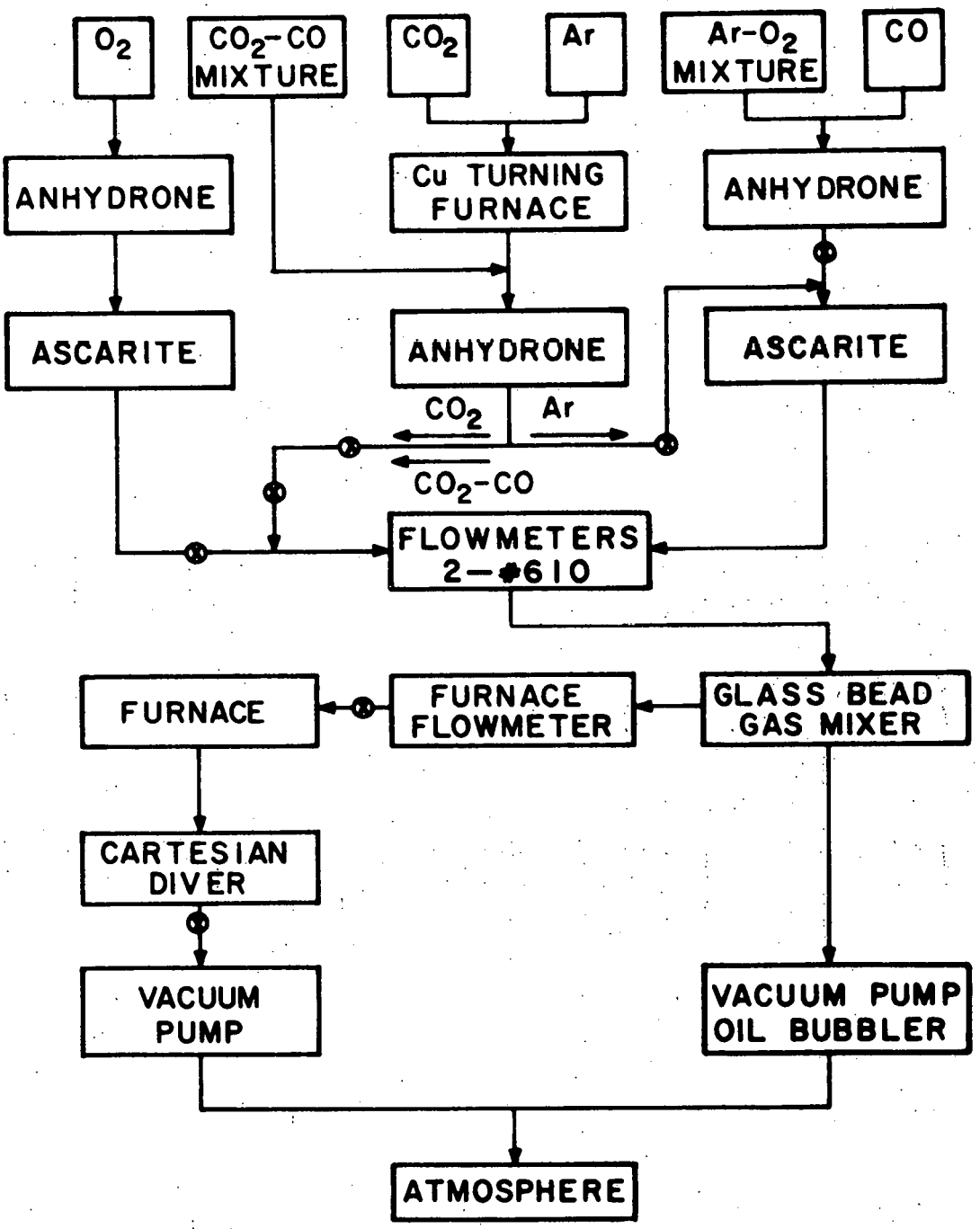

Figure 3. Diagram of gas purification, drying and control equipment.

established throughout the system. The time varied according to desired oxygen partial pressure with the longest times needed for the lowest oxygen partial pressures.

The oxygen partial pressure range in this study was $10^{-0.3}$ to $10^{-14.5}$ atm. Whenever possible the oxygen partial pressure was varied at 10^{-2} atm. intervals, but due to flow rate limitations and thermodynamic considerations this was not always possible at the lower temperatures.

Once the desired oxygen partial pressure was established, the furnace was heated to temperature. This would take from six to twelve minutes depending on how high a temperature was was desired. Once temperature was reached, weight gain measurements commenced. The temperature was maintained at ± 5°C of the desired experimental temperature. The temperature range investigated was 727-1327°C, at 150°C intervals.

After oxidation was completed, the gas flow was stopped and the furnace gradually cooled (ten to sixteen minutes). During cooling, the furnace was kept in place about the specimen to preserve the oxide coating. It was felt that immediate exposure to the air would be too much of a thermal shock causing the oxide to crack and drop off the quartz rod. Once the furnace was completely cooled, it was lowered and the oxidized specimen was removed from the quartz rod.

RESULTS AND DISCUSSION

Analysis Technique

Weight gain as a function of time was measured at each temperature for several controlled oxygen partial pressures. For each oxidation experiment the weight gain values were squared and plotted versus time (see Appendix for experimental data). The rational scaling rate constants were calculated from the slope of the best straight line portion of these plots at each temperature and oxygen partial pressure using Eq. 45, where $K_s = 1/t(\Delta W/A)^2$. All slopes were determined from a least-squares fit.

The values of K_r were plotted against $\ln P^{\circ}_{O_2}$ at each temperature. Equation 30 gives a relationship between the rational scaling rate constant, K_r, and the ionic conductivity, σ_{ionic}, when the oxide is behaving as a semiconductor. Differentiating Eq. 30 with respect to $\ln P^{\circ}_{O_2}$ yields

$$\frac{dK_r}{d \ln P^{\circ}_{O_2}} = \frac{kT}{4Fe} \sigma_{ionic} \Big|_{\ln P^{\circ}_{O_2}} \tag{48}$$

The left hand side of this equation may be evaluated by the slope of a least-squares fit of a straight line to the K_r versus $\ln P^{\circ}_{O_2}$ data. All values in Eq. 48 are now known except σ_{ionic} which can thus be calculated. Once a value for σ_{ionic} is known, the Nernst-Einstein equation permits calculation of self-diffusion coefficients for the oxygen ion.

A semilogarithmic plot of the self-diffusion coefficients versus reciprocal absolute temperature yielded a fit of the data to an Arrhenius equation of the type

$$D = D_o \exp\left(\frac{-Q}{RT}\right) \tag{49}$$

where

D_o = self-diffusion coefficient at $1/T = 0$ ($cm.^2/sec.$)

Q = activation energy (kcal./mole)

$-Q/R$ = slope of ln D vs 1/T plot

In the region where the oxide is behaving as an ionic conductor Eq. 33, if differentiated with respect to ln $P^{\circ}_{O_2}$, yields

$$\frac{dK_r}{d \ln P^{\circ}_{O_2}} = \frac{kT}{4Fe} \sigma_e \Big|_{\ln P^{\circ}_{O_2}} \tag{50}$$

A plot of K_r versus ln $P^{\circ}_{O_2}$ is the left side of Eq. 50. All values are known and σ_e was then calculated.

The parabolic rate constant, K_p, relates rate of increase in thickness of the oxide coating to time and is a useful piece of engineering data. These values were obtained from the K_r values using Eq. 40.

Experimental Results

The values for K_r, the rational scaling rate constant, are shown in Table 4. In general, the values for dysprosium were of greater magnitude, the greatest being nearly ten times the magnitude of that of gadolinium. Figures 4-12 show the

Table 4. Rational scaling rate constants (equivalents/cm.-sec.)

Temp. (°C)	P_{O_2}(atm.)	Gadolinium	Dysprosium
727	$10^{-0.3}$	2.482(x10^{11})	2.6520(x10^{10})
	$10^{-1.312}$	1.6980	1.5045
	$10^{-3.3}$	1.5020	1.2941
	$10^{-12.5}$	1.3066	1.2813
877	$10^{-0.3}$	1.1760(x10^{10})	3.2321(x10^{10})
	$10^{-1.342}$	0.8690	3.7995
	$10^{-3.3}$	1.0518	1.1028
	$10^{-8.6}$	0.4181	0.7395
	$10^{-14.5}$	0.3070	0.7458
1027	$10^{-0.3}$	1.6529(x10^{10})	4.6792(x10^{10})
	$10^{-1.342}$	0.6141	6.1008
	$10^{-3.3}$	1.0061	1.7276
	$10^{-5.6}$	0.7905	0.8032
	$10^{-11.6}$	0.4638	0.5928
	$10^{-13.6}$	0.7709	0.9371
1177	$10^{-0.3}$	2.9073(x10^{10})	2.5633(x10^{9})
	$10^{-1.342}$	2.0188	2.0635
	$10^{-3.3}$	0.8950	1.8787
	$10^{-9.3}$	0.8632	0.1842
	$10^{-11.3}$	0.9408	0.1090
1327	$10^{-0.3}$		3.6783(x10^{9})
	$10^{-1.342}$		2.9076
	$10^{-3.3}$		2.8719
	$10^{-7.3}$		1.7365
	$10^{-9.3}$		1.5574

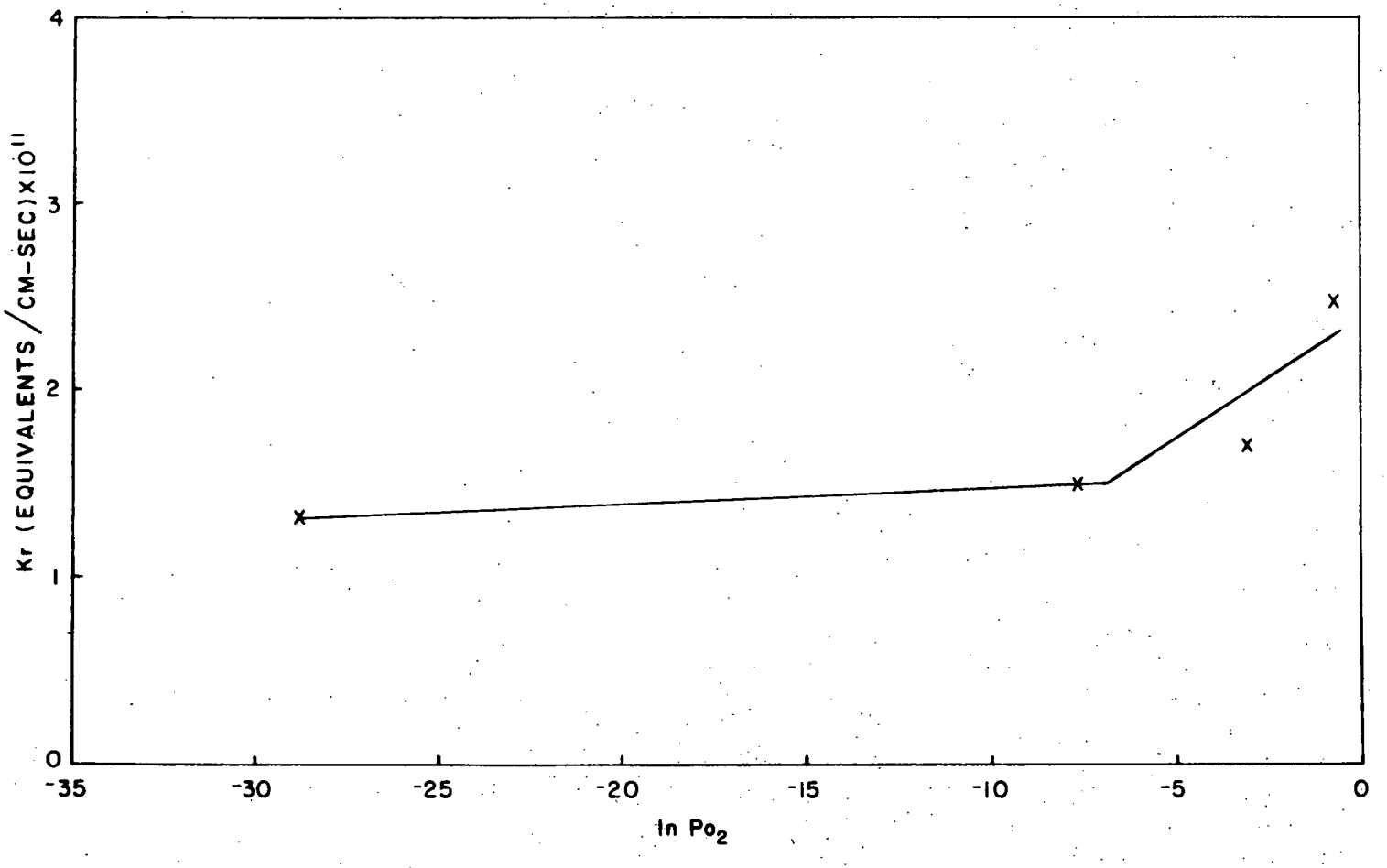

Figure 4. K_r vs. ln P_{O_2} for gadolinium at 727°C.

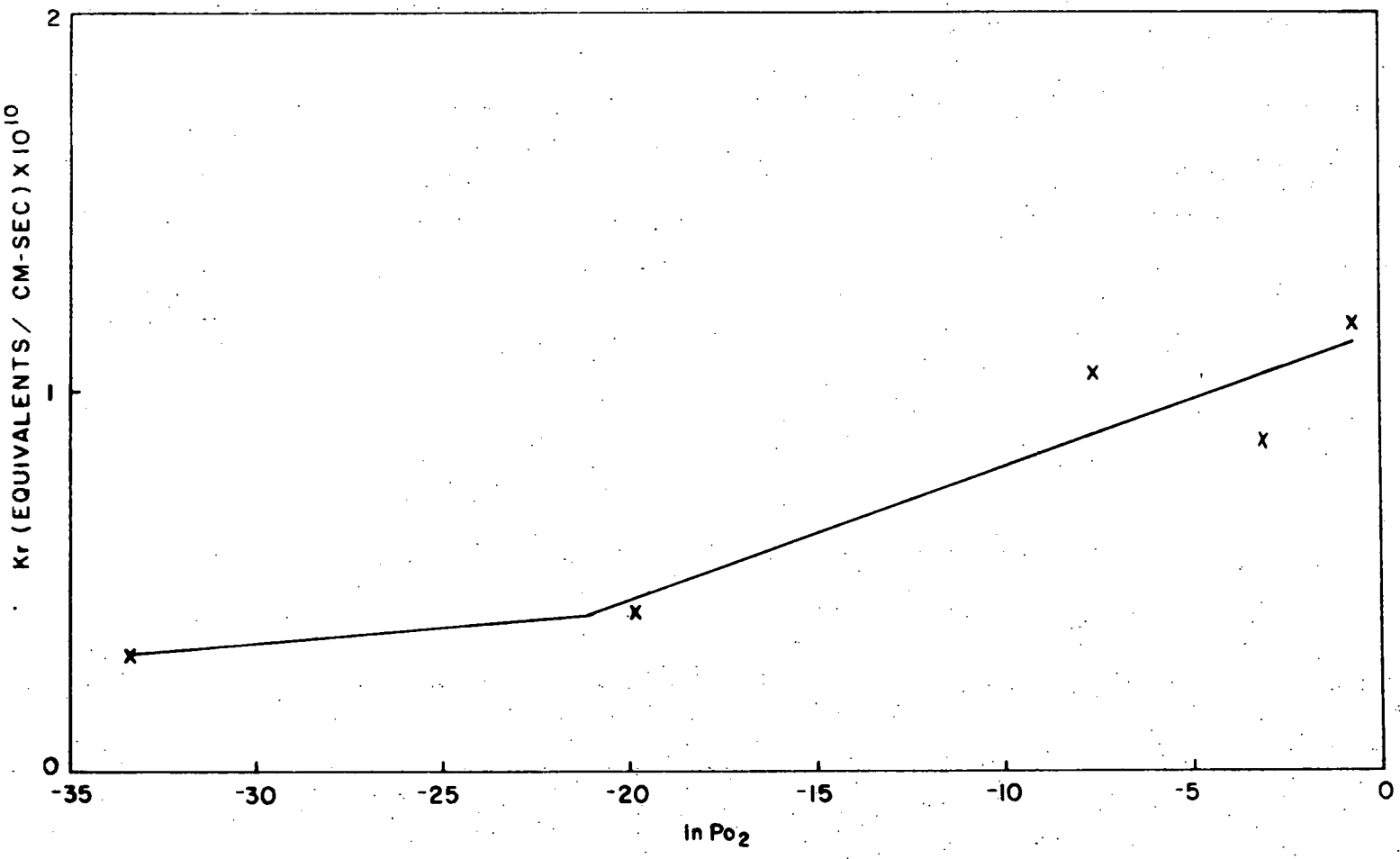

Figure 5. K_r vs. ln P_{O_2} for gadolinium at 877°C.

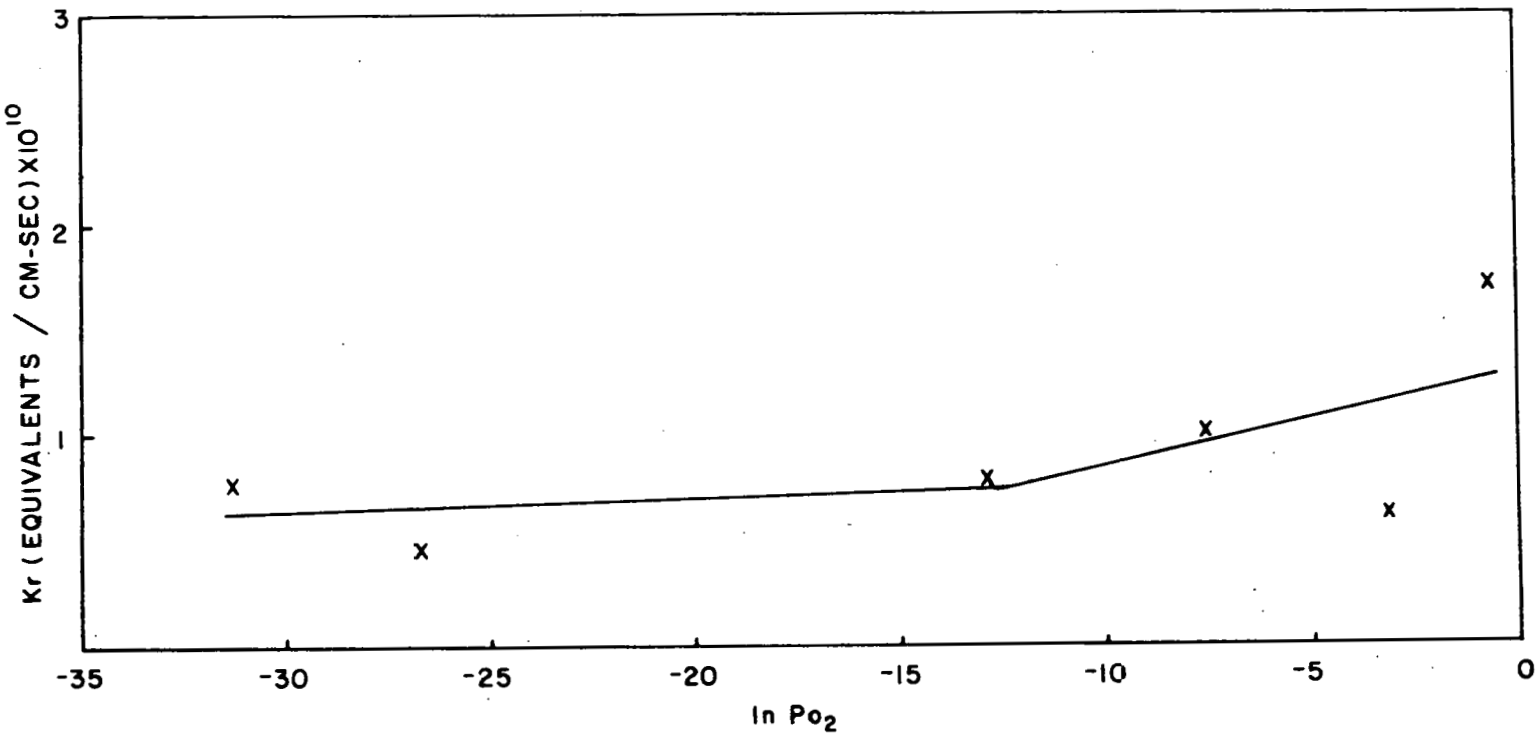

Figure 6. K_r vs. ln P_{O_2} for gadolinium at 1027°C.

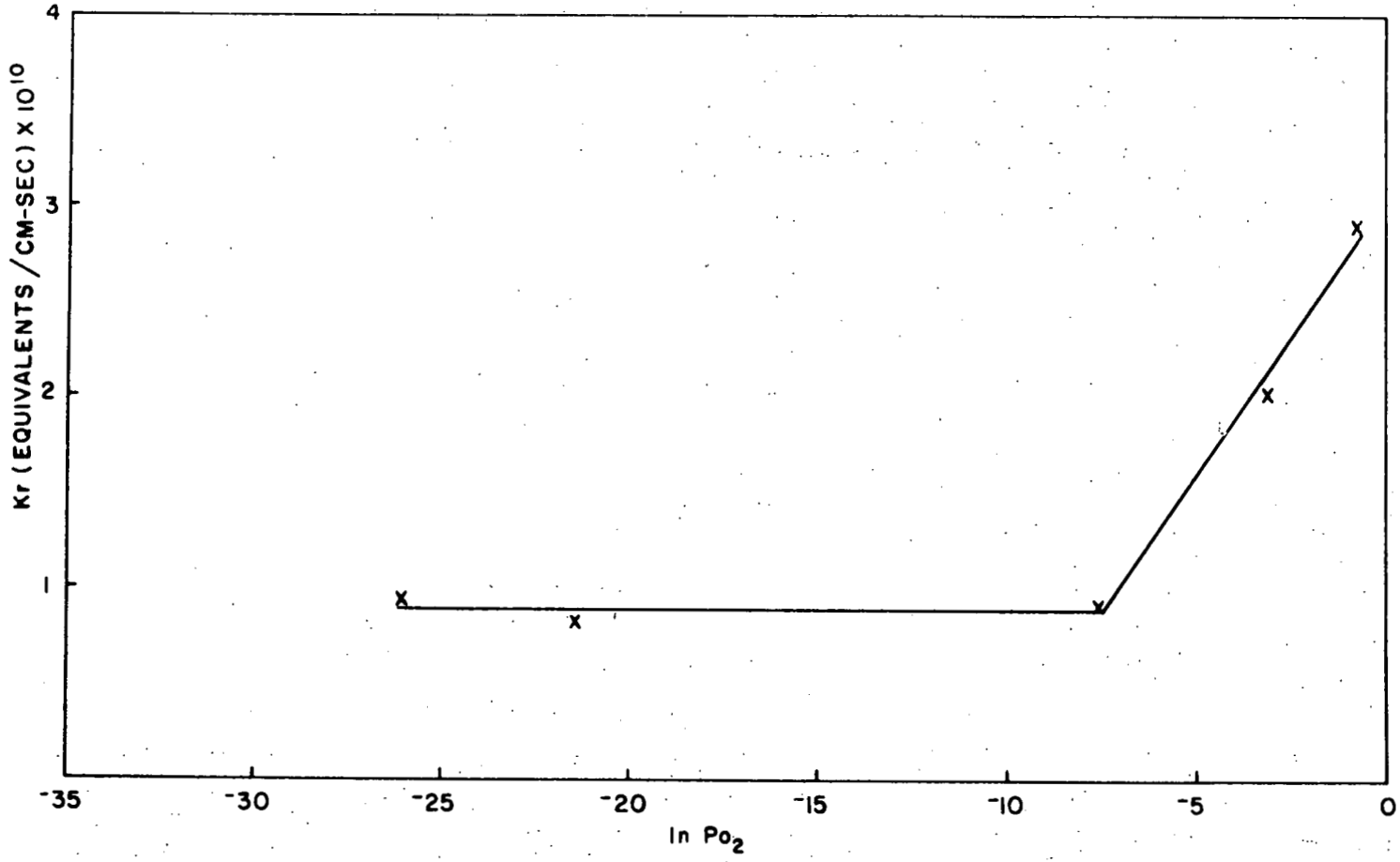

Figure 7. K_r vs. ln P_{O_2} for gadolinium at 1177°C.

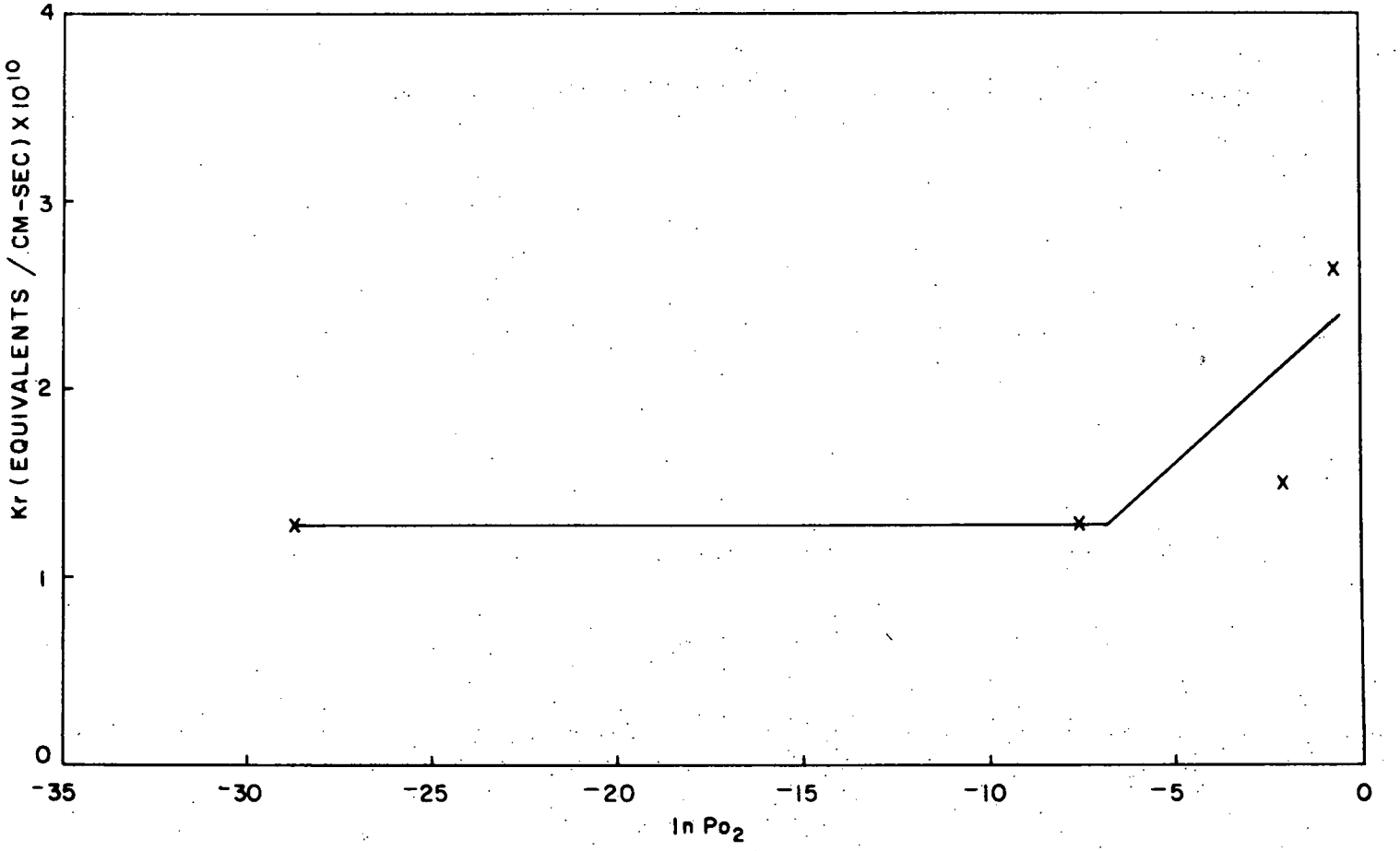

Figure 8. K_r vs. ln P_{O_2} for dysprosium at 727°C.

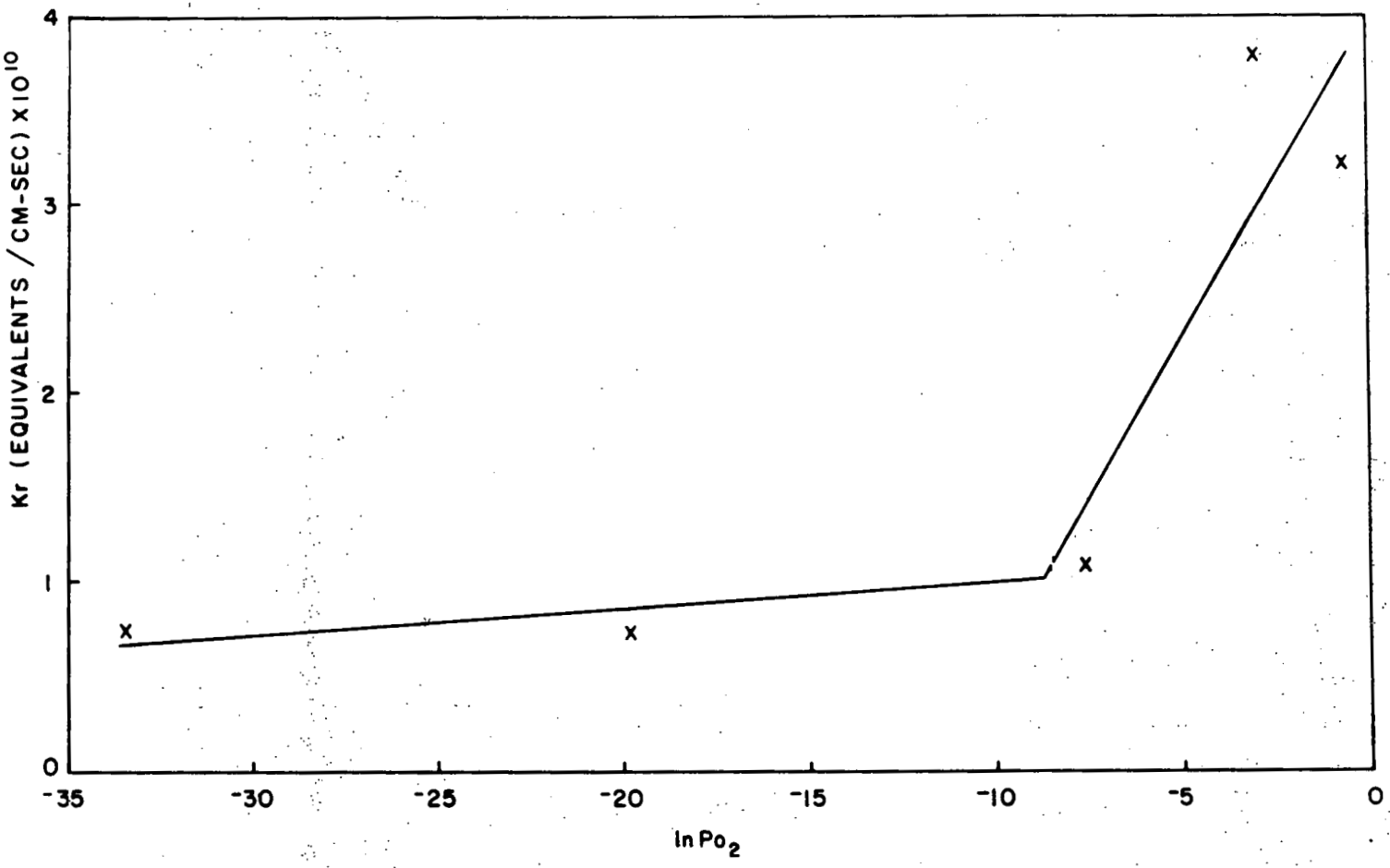

Figure 9. K_r vs. ln P_{O_2} for dysprosium at 877°C.

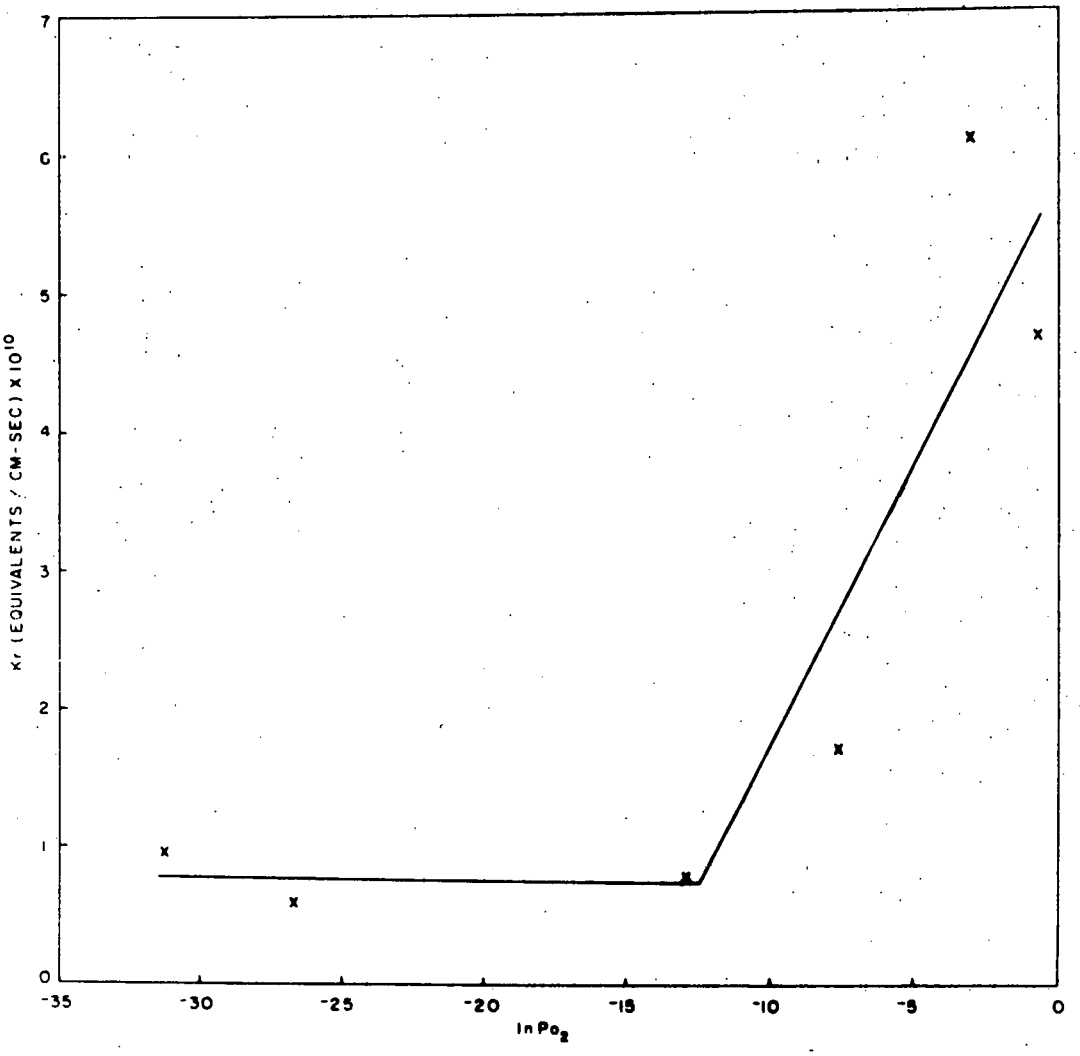

Figure 10. K_r vs. ln P_{O_2} for dysprosium at 1027°C.

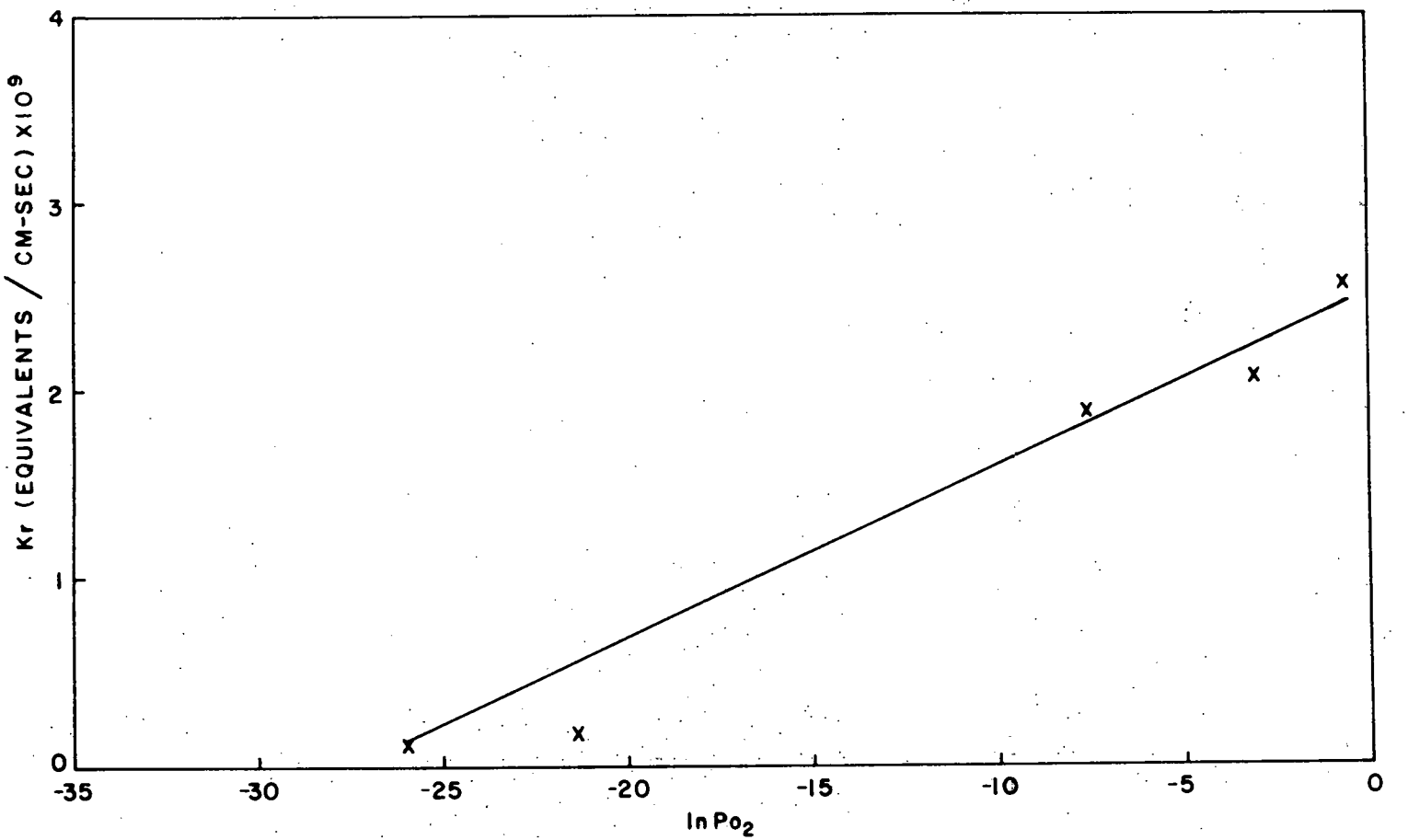

Figure 11. K_r vs. ln P_{O_2} for dysprosium at 1177°C.

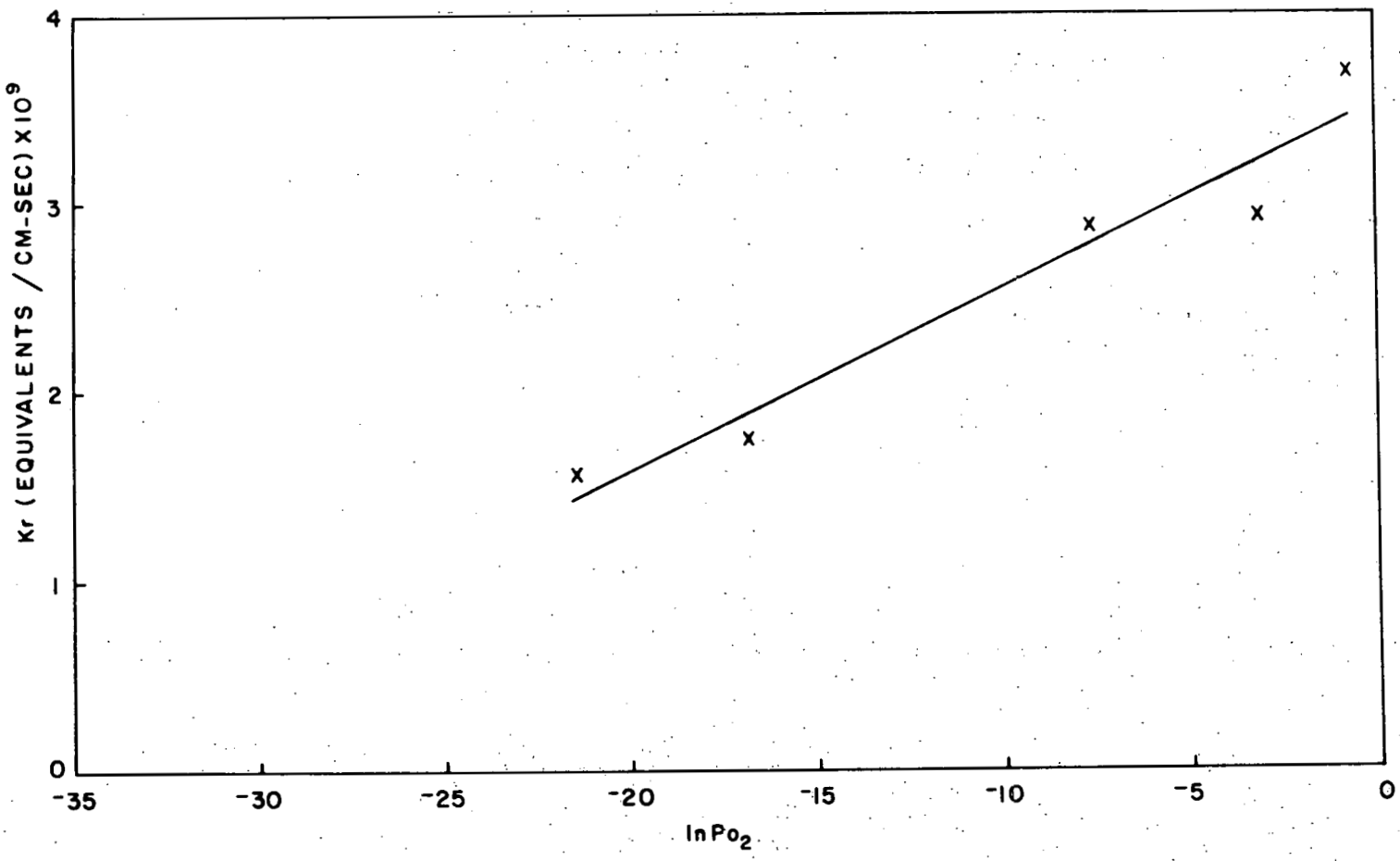

Figure 12. K_r vs. ln P_{O_2} for dysprosium at 1327°C.

K_r versus ln P_{O_2} curves for each metal and temperature. Macki (47) found, generally, two regions of conductivity as the oxygen partial pressure was varied from 10^0 to 10^{-20} atm. His study was used as a guideline in determining the straight line portions on Figures 4-12.

It is apparent from Figures 4-12 and Table 4 that there is some scatter and inconsistency in the data. For example, the rational scaling rate constant for dysprosium at 1027°C at an oxygen partial pressure of $10^{-1.342}$ atm. is higher than that at an oxygen partial pressure of $10^{-0.3}$ atm. It was expected that the rational scaling rate constant would decrease with decrease in oxygen partial pressure. Generally, this was true, but there were a few exceptions. Most oxidation runs at all temperatures and oxygen partial pressures were repeated, some even three times, and yet the results were nearly the same. A reason for this scatter was the difficulty in deciding the best straight line portion of the weight gain squared versus time curves. Often in the diffusion-controlled zone there were two or three straight line portions, each with a slightly different slope. The decision as to which was the best straight line was made by comparing the standard error of estimate of the least-square fits of the data. It was felt that the best straight line was that which had the lowest value (best fit) in the standard error of estimate. Therefore, for each oxygen partial pressure the slope used was from the best fit of the data to a straight line, but, due to this technique, scatter and inconsistency mentioned above still oc-

curred. It is this author's belief that the results obtained are the most accurate possible employing this technique.

As stated previously (see analysis technique section), when the oxide is behaving as a semiconductor the slope of a K_r versus ln $P^{\circ}_{O_2}$ curve will allow calculation of the self-diffusion coefficient of oxygen. Macki (47) studied the electrical conductivity of Gd_2O_3 and Dy_2O_3 as a function of oxygen partial pressure. He found that Gd_2O_3 generally was a p-type semiconductor above 10^{-10} atm. in the temperature range 800-1400°C. This study revealed that Gd_2O_3 was a p-type semi-conductor above $10^{-9.4}$ atm. in the temperature range 727-1177°C. Therefore, the slopes used for calculation of oxygen diffusion in Gd_2O_3 were those of the right hand portion of the curves in Figures 4-7.

The p-type semiconducting region in Dy_2O_3 found by Macki is above 10^{-8} atm. between 800 and 1400°C. This study found p-type semiconduction above $10^{-11.3}$ atm. in the temperature range of 727-1327°C. The slopes used for calculation of oxygen diffusion in Dy_2O_3 were the right hand portion of the curves in Figures 8-10. Figures 11 and 12, for 1177 and 1327 °C respectively, indicate apparent semiconduction throughout the entire experimental oxygen partial pressure range.

Conductivity studies were not done to substantiate that at high oxygen partial pressures the conduction was p-type semiconduction. Based on the positive slope and break observed in the K_r versus ln P_{O_2} curves and the study of Macki, it was inferred that the oxide scale is p-type semiconducting in

Gd_2O_3 over the oxygen partial pressure range above $10^{-9.4}$ atm. and above $10^{-11.3}$ atm. in Dy_2O_3.

Figures 13 and 14 present the oxygen diffusion coefficients in Gd_2O_3 and Dy_2O_3, respectively. As seen on Figure 13, the results of this study were compared to those of Wirkus et al. (48). They measured oxygen diffusion by measuring weight gain in slightly reduced gadolinium oxide ($GdO_{1.485}$) in air. The oxide was the monoclinic type B form. The data of Wirkus et al. fit an Arrhenius equation of the type

$$D = 5.87 \times 10^{-4} \exp\left(\frac{-28,800}{RT}\right) \qquad (51)$$

in the temperature range 750-1050°C. The data from this study on cubic Gd_2O_3 fit an Arrhenius equation of the type

$$D = 1.149 \times 10^{-7} \exp\left(\frac{-40,269}{RT}\right) \qquad (52)$$

From the work of Berard et al. (37) the cubic (C type) rare earth oxides tend to have lower oxygen diffusion coefficients than the monoclinic form of gadolinia. The diffusion coefficients in this study are lower than those of other oxides studied by Berard et al., but they did find some activation energies as high as the 40,269 cal./mole in this study.

Oxygen self-diffusion coefficients, in Dy_2O_3, as shown in Figure 14, were compared to those determined by Berard et al. (37). The data from this study fit an Arrhenius equation of the type

$$D = 2.831 \times 10^{-8} \exp\left(\frac{-21,393}{RT}\right) \qquad (53)$$

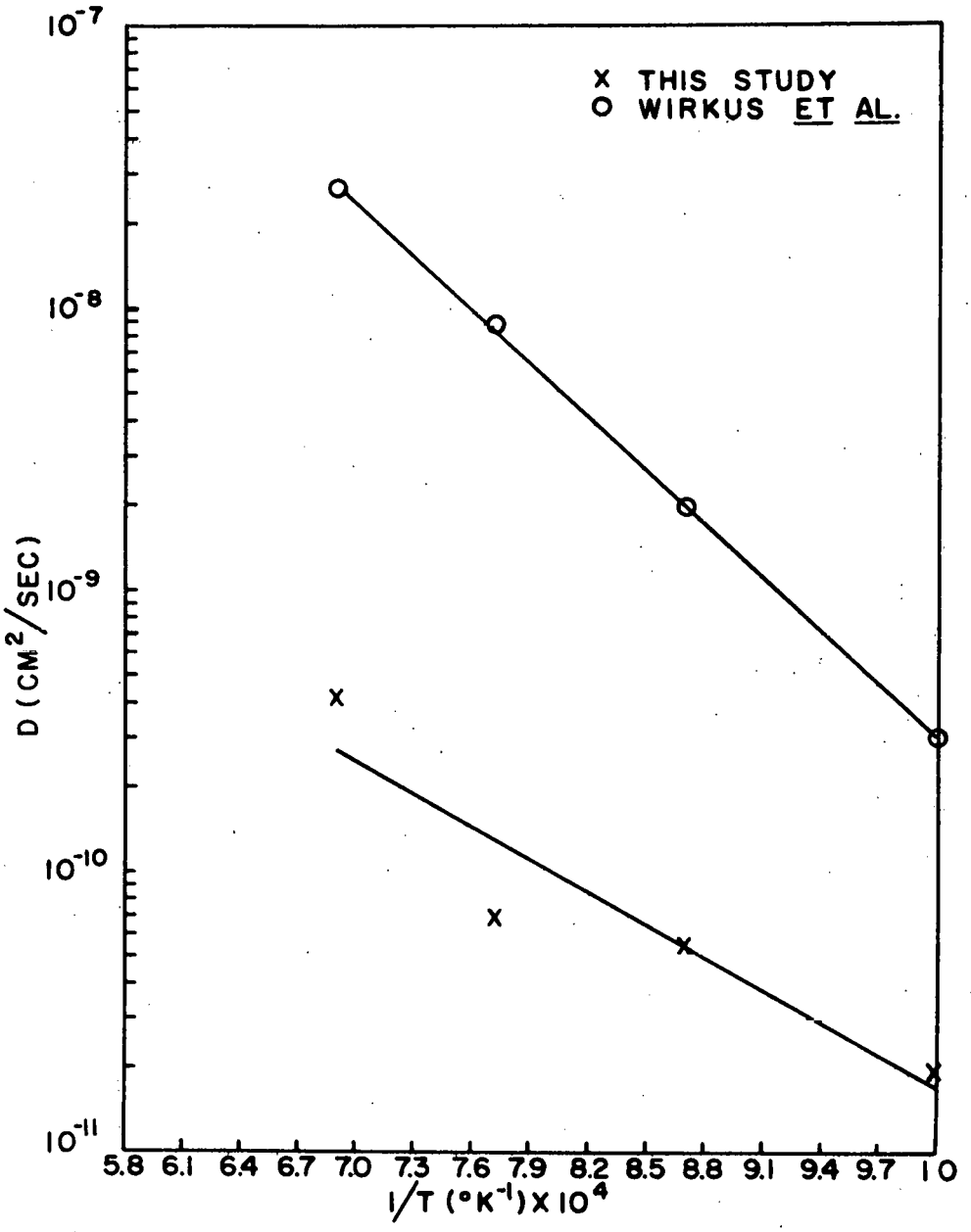

Figure 13. Oxygen diffusion coefficients in Gd_2O_3.

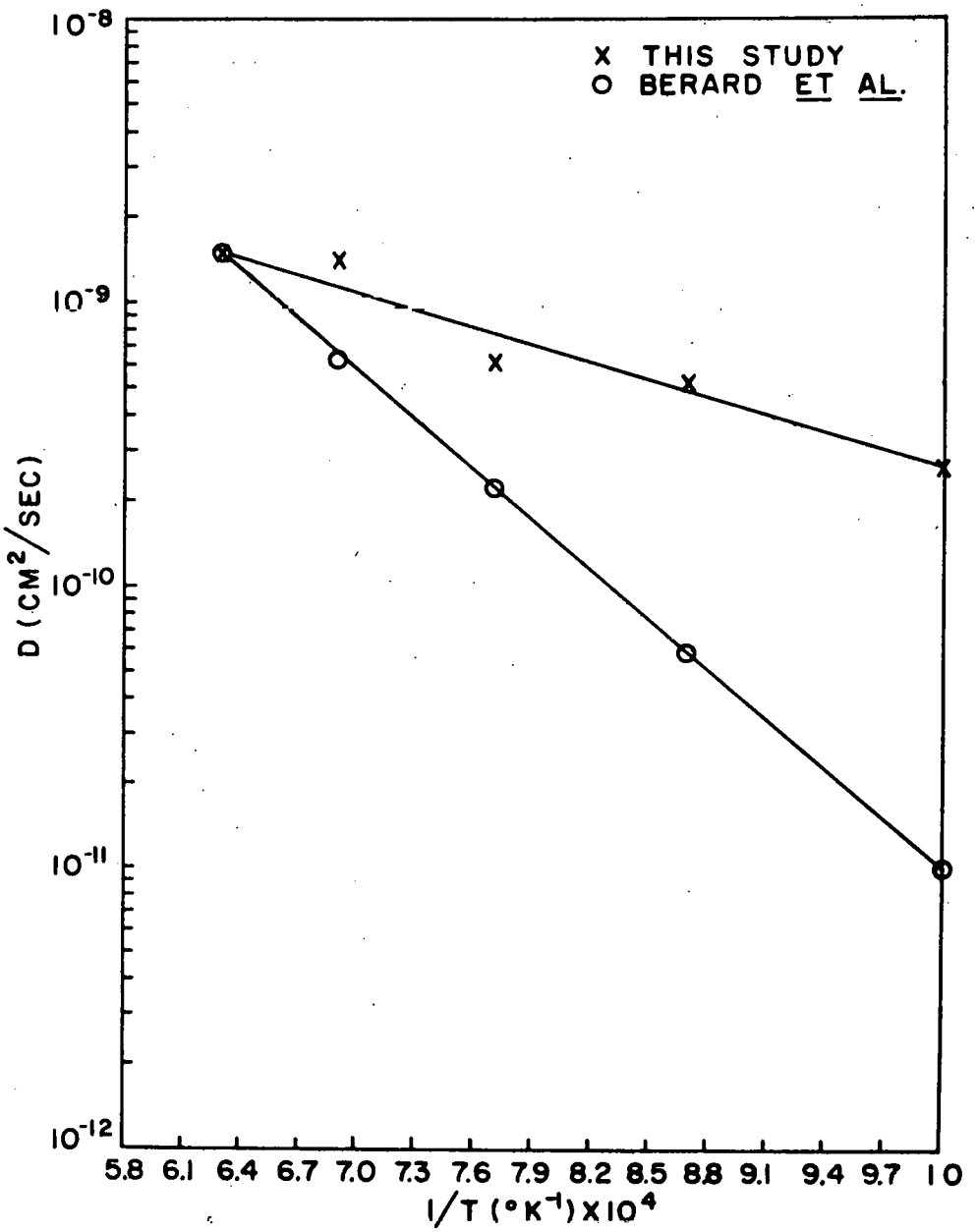

Figure 14. Oxygen diffusion coefficients in Dy_2O_3.

Berard et al., by measuring weight gain of a slightly reduced oxide, in the temperature range 1087-1235°C fitted their data to an Arrhenius equation of the type

$$D = 1.63 \times 10^{-5} \exp\left(\frac{-26,240}{RT} \right) \qquad (54)$$

The oxidation runs on gadolinium at 1027 and 1177°C and also for dysprosium at oxygen partial pressures of $10^{-9.3}$ and $10^{-11.3}$ atm. at a temperature of 1177°C were quite anomalous in their behavior. Figure 15 shows a representative specimen. The dark portion in the center is unoxidized metal. The white, grainy area is the oxide scale which is followed by the acrylic mounting material. These specimens when removed from the furnace had very little of the characteristic white oxide visible on the surface. Upon microscopic examination, the white oxide was found present on the interior of the specimen. The surface had the appearance of the reduced form of the oxide as shown by Berard et al. This is seen on Figure 15 as the thin, dark area between the white oxide and the acrylic mounting material. This anomalous oxidation behavior was exemplified in that the total amount of weight gain was significantly lower at these higher temperatures than at low temperatures for the same amount of time. Also, the time for apparently complete oxidation (time to reach a constant weight) did not show the expected exponential decrease from those at lower temperatures. Kofstad (32) states that oxidation reactions have shown empirically that the temperature dependence of oxidation rate constants obey an Arrhenius equation,

Figure 15. Gadolinium oxidized at T = 1027°C, $P_{O_2} = 10^{-3.3}$ atm. Sample polished and etched, 350X.

Figure 16. Dysprosium oxidized at T = 1327°C, $P_{O_2} = 10^{-9.3}$ atm. Sample polished and etched, 350X.

THIS PAGE
WAS INTENTIONALLY
LEFT BLANK

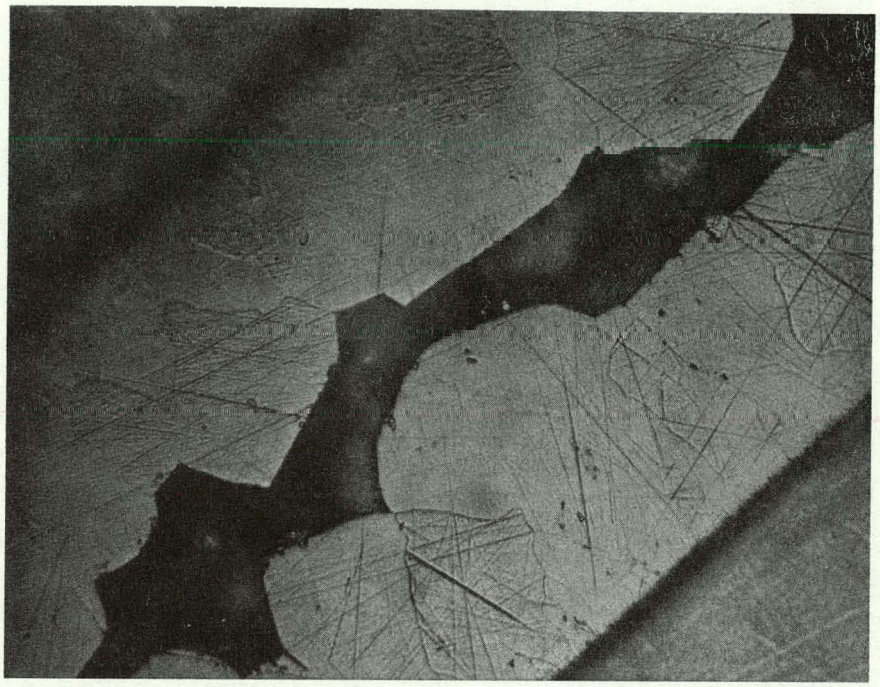

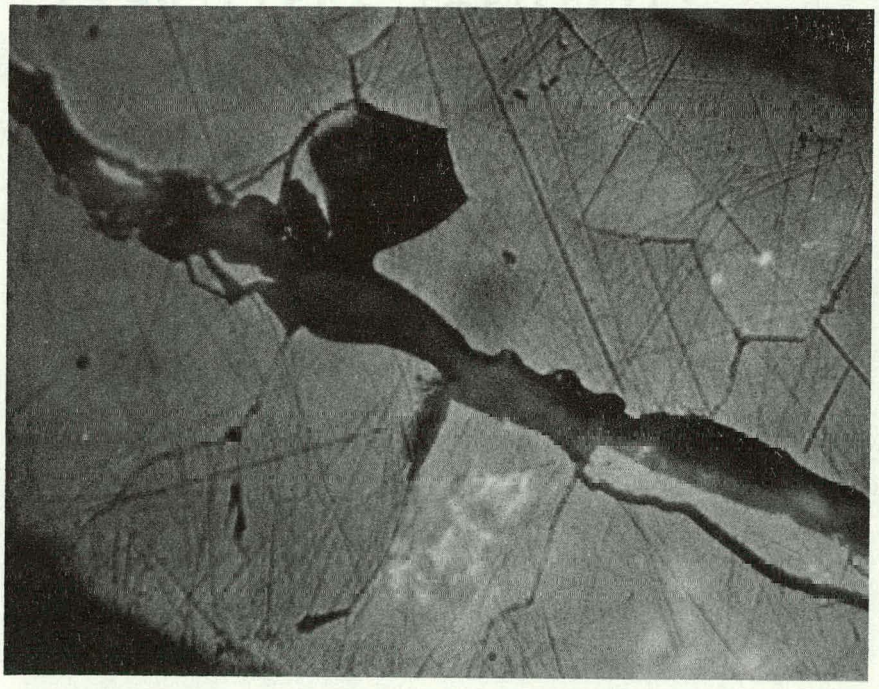

$K = K_o \exp(-Q/RT)$. Therefore, since the rate constant will exponentially increase with temperature, time will exponentially decrease with temperature. The presence of unoxidized metal is consistent with less than expected total weight gain.

Figures 15 and 16 show large grains and the presence of compact and protective oxide scale which was an assumption made to allow use of the Wagner analysis (25) in this type of study. Figure 16 is representative of the oxidation of dysprosium at 1327°C. All that is visible in Figure 16 is the white oxide scale and the acrylic mounting material. The dark portion in the center of the micrograph is a separation in the oxide scale and and not unoxidized metal. Only at this temperature did the diffusion coefficient agree with that of Berard et al. (37).

Figure 17 exemplifies the oxide microstructure on all of the other oxidation experiments on both metals. The specimen was polished then etched before observation with the scanning electron microscope. There is the presence of many small grains, but there are many holes in the oxide scale. It appears that a porous oxide scale may have been formed and, thereofre, possibly the Wagner analysis (25) does not give a complete description of the oxidation process at these lower temperatures. Also, the presence of a porous scale would yield higher than expected diffusion coefficients as was the case for dysprosium except at 1327°C. The presence of porosity allows for the reaction of the metal and gaseous oxygen

Figure 17. Scanning electron micrograph of gadolinium oxidized at T = 877°C, $P_{O_2} = 10^{-8.6}$ atm. Sample etched, 3000X.

to occur directly at the metal/oxide interface without diffusion of oxygen through the oxide scale. The weight gain measured would be higher than that if the oxide scale were completely protective, thus, this leads to a higher scaling rate constant. With a greater value for scaling rate constant the calculated diffusion coefficient would then be greater.

Kofstad (32) states that when oxygen moves inward, as in this study, it may generally be expected that larger stresses are developed in the oxide scale than when the metal moves outward. These stresses tend to rupture the oxide scale after it has reached a certain critical thickness. This rupture of the oxide scale would tend to leave a porous, nonprotective oxide scale and the Wagner analysis would not give a complete description of the oxidation process.

With the presence of small grains, grain boundary diffusion may have had some importance. Kofstad states that grain boundary diffusion will as a rule be significant at temperatures below the Tamman temperature (two-thirds of the absolute melting point). This study was carried out in that region. The activation energy would probably be less for grain boundary diffusion than for volume diffusion. These arguments may give some basis for the higher diffusion coefficients in Dy_2O_3 found in this study than those presented by Berard et al. (37).

However, there is some cause to think that there may have been a coherent, protective scale present on the lower

temperature Dy_2O_3 runs. A difficulty in this method is the necessity of after-the-fact microscopic examination. On several runs before completion there were losses of weight followed by rapid gain in weight. Possibly in the later stages of oxidation the scale thickness became too great for the specimen size and some of the oxide fell off leaving a nonprotective, porous scale which was later observed microscopically. The good possibility that a protective scale was present during the stages of oxidation when scaling rates were determined means that the diffusion coefficients obtained here are quite possibly correct. The fact that these coefficients are larger than those previously reported by Berard et al. may be due to maximum solubility assumptions made in the earlier study which resulted in coefficients which may be low.

As seen in Figure 17, the oxide scale formed on gadolinium at lower temperatures appears to be quite porous, thus, the possibility of the presence of a nonprotective oxide scale. This would lead to the conclusion that the diffusion coefficients would be higher than reported by Wirkus et al. (48). However, the diffusion coefficients found in this study are lower. For the reasoning given in the previous paragraph, there may have been a coherent, protective scale present when scaling rates were determined, thus, the diffusion coefficients obtained here are quite possibly correct.

The rational scaling rate constants can be converted to

Table 5. Parabolic rate constants ($cm.^2/sec.$)

Temp. (°C)	P_{O_2}(atm.)	Gadolinium($x10^{10}$)	Dysprosium($x10^{10}$)
727	$10^{-0.3}$	2.025	2.111
	$10^{-1.342}$	1.385	1.198
	$10^{-3.3}$	1.225	1.030
	$10^{-12.5}$	1.066	1.020
877	$10^{-0.3}$	9.592	2.573
	$10^{-1.342}$	7.088	3.024
	$10^{-3.3}$	8.579	0.878
	$10^{-8.6}$	3.410	0.589
	$10^{-14.5}$	2.504	0.594
1027	$10^{-0.3}$	13.482	3.725
	$10^{-1.342}$	5.009	4.856
	$10^{-3.3}$	8.206	1.375
	$10^{-5.6}$	6.448	0.639
	$10^{-11.6}$	3.783	0.472
	$10^{-13.6}$	6.288	0.746
1177	$10^{-0.3}$	23.714	20.404
	$10^{-1.342}$	16.467	16.425
	$10^{-3.3}$	7.300	14.954
	$10^{-9.3}$	6.715	1.466
	$10^{-11.3}$	7.674	0.868
1327	$10^{-0.3}$		29.279
	$10^{-1.342}$		23.144
	$10^{-3.3}$		22.860
	$10^{-7.3}$		13.822
	$10^{-9.3}$		12.397

parabolic rate constants, which are of more value in engineering usage, by means of Eq. 40. The parabolic rate constants for each temperature and oxygen partial pressure are given in Table 5.

As previously discussed, when the oxide is behaving as an ionic conductor it is possible to calculate the electronic conductivity values from the slope of the K_r versus ln P_{O_2} curve. For these values the nearly straight line portions of Figures 4-12 were used. The slopes were derived from a least squares fit of the data. Table 6 gives the electronic conductivity values including one standard deviation. Due to scatter, two negative values of electronic conductivity were found. Since the standard deviation in these cases is of greater magnitude than the calculated conductivity, the reason for the negative value may be explained.

Table 6. Electronic conductivity (1/ohm-cm.)

Temperature (°C)	Gadolinium	Dysprosium
727	4.115×10^{-7}[a]	2.604×10^{-7}[a]
877	3.151×10^{-6}[a]	$5.250 \pm 3.35) \times 10^{-6}$
1027	$(2.133 \pm 6.15) \times 10^{-6}$	$(-6.880 \pm 61.2) \times 10^{-7}$
1177	$(-2.159 \pm 18.5) \times 10^{-7}$	

[a]Insufficient data to calculate standard deviation.

CONCLUSIONS

1. The self-diffusion coefficient of oxygen in cubic Gd_2O_3 in the temperature range of 727-1177°C fits the following Arrhenius equation:

$$D = 1.149 \times 10^{-7} \exp\left(\frac{-40,269}{RT}\right)$$

2. The self-diffusion coefficient of oxygen in cubic Dy_2O_3 in the temperature range of 727-1327°C fits the following Arrhenius equation:

$$D = 2.831 \times 10^{-8} \exp\left(\frac{-21,393}{RT}\right)$$

3. In the temperature range 727-1177°C, the shape of the K_r versus ln P_{O_2} plots is consistent with p-type semiconduction in Gd_2O_3 above $10^{-9.4}$ atm.

4. In the temperature range 727-1327°C, the shape of the K_r versus ln P_{O_2} plots is consistent with p-type semiconduction in Dy_2O_3 above $10^{-11.3}$ atm.

5. The technique employed in this study to measure self-diffusion of oxygen in rare earth oxides may not be entirely accurate. Parabolic oxidation does occur, but there is not conclusive evidence that at all temperatures a coherent, protective oxide scale forms on the metal surface. Thus, the Wagner analysis may not completely describe the oxidation behavior of the rare earth oxides.

BIBLIOGRAPHY

1. T. Moeller; pp. 9-28 in The Rare Earths. Edited by F. H. Spedding and A. H. Daane. John Wiley and Sons, Inc., New York, 1961.

2. J. A. Gibson and G. S. Harvey, "Properties of the Rare Earth Metals and Compounds," Tech. Rept. AFML-TR-65-430, Air Force Materials Laboratory, January, 1966.

3. A. H. Daane; p. 179 in The Rare Earths. Edited by F. H. Spedding and A. H. Daane. John Wiley and Sons, Inc., New York, 1961.

4. J. Loriers, "Sur l'oxydation du cérium et du lanthane," Academie des Sciences Comptes Rendus, 229 [11] 547-49 (1949).

5. N. D. Greene and F. G. Hodge, "Oxidation Characteristics of the Lanthanide Metals," Corrosion, 22 [7] 206-13 (1966).

6. W. L. Phillips, Jr., "Oxidation of Several Lanthanide Elements," J. Less-Common Metals, 7, 139-43 (1964).

7. L. Lee and N. D. Greene, "Corrosion Characteristics of the Rare Earth and Yttrium Metals," Corrosion, 20 [5] 145t-49t (1964).

8. B. Love, "Selection and Reduction of Rare or Unusual Metals. Part II. The Metallurgy of Yttrium and the Rare Earth Metals," Tech. Rept. WADC-TR-57-666, Part II, Wright Air Development Center, 1959.

9. K. S. Vorres, "A Kinetic Study of the Oxidation of Rare Earth Metals, Solubility of Rare Earth Metals in Their Nitrides, and Infra-Red Studies on Some Rare Earth Compounds," Ph.D. Thesis, State University of Iowa, Iowa City, Iowa, 1958.

10. K. S. Vorres and L. Eyring, pp. 119-123 in Rare Earth Research. Edited by E. V. Kleber. The Macmillan Co., New York, 1961.

11. W. Edmondson, K. Goodhead, and P. M. S. Jones, "The Oxidation of Rare Earth Metals. Part 1. Bulk Materials," Tech. Rept. AWRE 0-45/64, Atomic Weapons Research Establishment, Great Britian, July, 1964.

12. W. L. Phillips, Jr., "Some Observations on the High Temperature Oxidation of Lanthanum," J. Electrochem. Soc., 111 [10] 1184-85 (1964).

13. L. D. Pethe, H. B. Mathur, and A. B. Biswas, "High Temperature Oxidation Kinetics of Lanthanum Metal," Indian J. Chem., 5, 427-29 (1967).

14. J. Loriers, "Loi d'oxydation du cérium métallique. Généralisation à d'autre métaux," Academie des Sciences Comptes Rendus, 231 [10] 522-24 (1950).

15. D. Cubicciotti, "The Reaction of Cerium with Oxygen," J. Amer. Chem. Soc., 74 [5] 1200-01 (1952).

16. V. B. Glushkova, Yu. G. Sokolov, and E. K. Keler, "Oxidation of Metallic Neodymium and the Rate of the C→A Polymorphic Transformation of Neodymium Trioxide," Russ. J. Phys. Chem., 38 [5] 615-20 (1964).

17. H. J. Borchardt, "On the Oxidation of Yttrium," J. Inorg. Nucl. Chem., 26, 711-19 (1964).

18. J. A. Haefling, F. A. Schmidt, and O. N. Carlson, "Air Oxidation of Yttrium and Some Yttrium-Base Alloys," J. Less-Common Metals, 7, 433-40 (1964).

19. O. N. Carlson, F. A. Schmidt, and R. L. Wells, "A Study of the High-Temperature Air Oxidation of Yttrium Metal," Tech. Rept. IS-115, Institute for Atomic Research, Iowa State University, 1966.

20. S. A. D'Souza, H. B. Mathur, and A. B. Biswas, "Oxidation of Gadolinium in the Temperature Range 500-700°C," Indian J. Chem., 2, 307-11 (1964).

21. L. D. Pethe, H. B. Mathur, and A. B. Biswas, "Kinetics of Oxidation of Dysprosium Metal in the Temperature Region 500-800°C," Indian J. Chem., 6, 156-58 (1968).

22. T. J. Rider, "Kinetics of the Oxidation of Thulium by Oxygen and Water Vapor," M.S. Thesis, Iowa State University, Ames, Iowa, 1966.

23. J. Brett and L. Seigle, "Diffusion-Controlled Oxidation of Several Lanthanides," J. Less-Common Metals, 10, 22-28 (1966).

24. M. Foex and J. P. Traverse, "Remarques sur les Transformations Cristallines Présentées a Hautes Température par

les Sesquioxydes de Terres Rares," Rev. Int. Hautes Temp. Refract., 3 [4] 429-53 (1966).

25. C. Wagner, "Contribution to the Theory of the Oxidation Process," Z. Phys. Chem., 21 [1-2] 25-41 (1933).

26. N. B. Pilling and R. E. Bedworth, "The Oxidation of Metals at High Temperatures," J. Inst. Metals, 29 [1] 529-37 (1923).

27. T. P. Hoar and L. E. Price, "The Electrochemical Interpretation of Wagner's Theory of Tarnishing Reactions," Trans. Faraday Soc., 34, 867-72 (1938).

28. H. A. Miley, "Theory of Oxidation and Tarnishing of Metals. I. The Linear, Parabolic and Logarithmic Laws," Trans. Electrochem. Soc., 81, 391-403 (1942).

29. O. H. Hamilton and H. A. Miley, "Theory of Oxidation and Tarnishing of Metals. II. Growth Laws Under More General Conditions," Trans. Electrochem. Soc., 81, 413-21 (1942).

30. T. B. Grimley, pp. 336-366 in Chemistry of the Solid State. Edited by W. E. Garner. Academic Press, Inc., New York, 1955.

31. A. U. Seybolt, "Oxidation of Metals," Advan. Phys., 12 [45] 1-43 (1963).

32. P. Kofstad, High Temperature Oxidation of Metals. John Wiley and Sons, Inc., New York, 1966.

33. K. Hauffe, Oxidation of Metals. Plenum Press, New York, 1965.

34. O. Kubaschewski and B. E. Hopkins, Oxidation of Metals and Alloys, 2d ed. Academic Press, Inc., New York, 1962.

35. K. Hauffe, pp. 282-293 in Kinetics of High Temperature Processes. Edited by W. D. Kingery. John Wiley and Sons, Inc., New York, 1959.

36. L. Heyne, pp. 149-164 in Mass Transport of Oxides. Edited by J. B. Wachtman, Jr., and A. D. Franklin. Nat. Bur. Stand. U.S. Spec. Publ. 296, 1968.

37. M. F. Berard, C. D. Wirkus, and D. R. Wilder, "Diffusion of Oxygen in Selected Monocrystalline Rare Earth Oxides," J. Amer. Ceram. Soc., 51 [11] 643-47 (1968).

38. R. S. Roth and S. J. Schneider, "Phase Equilibria in Systems Involving the Rare-Earth Oxides. Part 1. Polymorphism of the Oxides of the Trivalent Rare-Earth Ions," J. Res. Nat. Bur. Stand., 64A [4] 309-16 (1960).

39. I. Warshaw and R. Roy, "Polymorphism of the Rare Earth Sesquioxides," J. Phys. Chem., 65 [11] 2048-51 (1961).

40. M. W. Shafer and R. Roy, "Rare-Earth Polymorphism and Phase Equilibria in Rare-Earth Oxide-Water Systems," J. Amer. Ceram. Soc., 42 [11] 563-70 (1959).

41. V. B. Glushkova and A. G. Boganov, "Polymorphism of Rare-Earth Sesquioxides," Bull. Acad. Sci. USSR, Chem. Ser., 1101-07 (1965).

42. V. M. Goldschmidt, F. Ulrich, and T. Barth, "Geochemical Distribution of the Elements. IV. On the Crystal Structure of the Oxides of the Rare Earth Metals," Skrifter Norske Videnskaps-Akad. Oslo I. Mat. Naturv. Kl., No. 5, 1925.

43. V. S. Rudenko and A. G. Boganov, "Nature of Irreversible Polymorphic Transformations of Rare Earth Oxides," Tech. Rept. LA-4169-TR, Los Alamos Scientific Laboratory, September 15, 1969.

44. S. Stecura, "Crystallographic Modifications and Kinetics of Phase Transformations of La_2O_3, Nd_2O_3, Sm_2O_3, Eu_2O_3, and Gd_2O_3," Ph.D. Thesis, Georgetown University, Washington, D.C., 1964.

45. C. E. Wicks and F. E. Block, "Thermodynamic Properties of 65 Elements - Their Oxides, Halides, Carbides, and Nitrides," Bur. Mines Bull. 605, Dept. of Interior, United States Gov. Print. Office, 1963.

46. A. Levy, "The Accuracy of the Bubble Meter Method for Gas Flow Measurements," J. Sci. Instrum., 41, 449-53 (1964).

47. J. M. Macki, "The Electrical Conductivity of Pure and Doped Dy_2O_3 and Gd_2O_3," Ph.D. Thesis, Ohio State University, Columbus, Ohio, 1968.

48. C. D. Wirkus, M. F. Berard, and D. R. Wilder, "Oxygen Diffusion in Gd_2O_3," J. Amer. Ceram. Soc., 52 [8] 456 (1969).

ACKNOWLEDGEMENTS

The author wishes to express sincere appreciation and gratitude to his major professor, Dr. Michael F. Berard, for advice, guidance, and encouragement during the course of this study; to Mr. C. D. Wirkus for advice and expertise in the use of the Cahn RG Electrobalance; to Verna Thompson for the typing of this thesis; and to my wife, Carolyn, for her patience, encouragement, and understanding during our stay at Iowa State.

APPENDIX. EXPERIMENTAL DATA

Table A1. Experimental data for gadolinium

Temp. °C	P_{O_2} (atm.)	ln P_{O_2}	[Weight gain]^2 (mg.^{2})	Time (min.)
727	$10^{-0.3}$	-0.690	18.455	960
			18.558	980
			18.662	1000
			18.731	1020
			18.627	1040
			18.809	1060
			18.731	1080
			18.844	1100
			19.245	1120
			19.210	1140
	$10^{-1.342}$	-3.090	25.694	920
			25.806	940
			26.050	960
			26.050	980
			26.101	1000
			25.908	1020
			26.050	1040
			25.979	1060
			26.255	1080
			26.327	1100
			26.512	1120
			26.357	1140
			26.399	1160
			26.357	1180
			26.337	1200
			26.594	1220
			26.822	1240
	$10^{-3.3}$	-7.599	17.355	880
			17.522	900
			17.447	920
			17.447	940
			17.707	960
			17.606	980
			17.614	1000
			17.673	1020
			17.833	1040
			17.960	1060
			17.816	1080
			18.003	1100
			17.875	1120
			17.918	1140
			17.875	1160

Table A1. (Continued)

Temp. °C	P_{O_2}(atm.)	ln P_{O_2}	[Weight gain]^2(mg.^{2})	Time (min.)
727	$10^{-3.3}$	-7.599	17.901	1180
			18.088	1200
			18.421	1220
			18.275	1240
			18.326	1260
	$10^{-12.5}$	-28.787	17.032	1000
			17.056	1020
			17.106	1040
			17.181	1060
			17.205	1080
			17.222	1100
			17.272	1120
			17.280	1140
			17.380	1160
877	$10^{-0.3}$	-0.690	12.652	360
			13.032	380
			13.293	400
			13.741	420
			14.107	440
			14.508	460
			14.768	480
	$10^{-1.342}$	-3.090	15.586	520
			15.888	540
			16.152	560
			16.451	580
			16.662	600
			16.932	620
	$10^{-3.3}$	-7.599	18.249	560
			18.550	580
			18.861	600
			19.219	620
	$10^{-8.6}$	-19.805	21.224	260
			21.344	280
			21.511	300
			21.650	320
			21.734	340
			21.930	360
			21.967	380

Table A1. (Continued)

Temp. °C	P_{O_2} (atm.)	ln P_{O_2}	[Weight gain]^2 (mg.^{2})	Time (min.)
877	$10^{-14.5}$	-33.343	2.666	460
			2.755	480
			2.873	500
			2.944	520
			3.055	540
			3.139	560
			3.225	580
			3.341	600
1027	$10^{-0.3}$	-0.690	5.373	260
			5.875	280
			6.290	300
			6.890	320
			7.398	340
	$10^{-1.342}$	-3.090	2.277	180
			2.455	200
			2.676	220
			2.842	240
			3.038	260
			3.218	280
	$10^{-3.3}$	-7.599	5.299	260
			5.640	280
			5.973	300
			6.165	320
			6.497	340
			6.848	360
			7.182	380
			7.474	400
			7.778	420
			8.105	440
			8.444	460
			8.649	480
			9.024	500
			9.363	520
			9.597	540
			9.897	560
			10.208	580
			10.575	600
			10.870	620

Table A1. (Continued)

Temp. °C	P_{O_2}(atm.)	ln P_{O_2}	[Weight gain]^2(mg.^{2})	Time (min.)
1027	$10^{-5.6}$	-12.896	6.543	400
			6.760	420
			7.080	440
			7.290	460
			7.491	480
	$10^{-11.6}$	-26.715	2.280	280
			2.421	300
			2.588	320
			2.732	340
			2.862	360
			2.985	380
			3.143	400
	$10^{-13.6}$	-31.321	2.458	260
			2.666	280
			2.900	300
			3.139	320
			3.385	340
			3.632	360
1177	$10^{-0.3}$	-0.690	9.504	140
			10.497	160
			11.397	180
			12.285	200
			13.060	220
	$10^{-1.342}$	-3.090	15.689	180
			16.467	200
			17.056	220
			17.556	240
	$10^{-3.3}$	-7.599	3.186	180
			3.407	200
			3.697	220
			3.988	240
			4.268	260
	$10^{-9.3}$	-21.417	2.819	220
			3.073	240
			3.294	260
			3.523	280
			3.802	300
			4.100	320

Table A1. (Continued)

Temp. °C	P_{O_2} (atm.)	ln P_{O_2}	[Weight gain]^2 (mg.^{2})	Time (min.)
1177	$10^{-11.3}$	-26.023	6.832	360
			7.139	380
			7.414	400
			7.695	420
			7.986	440
			8.236	460
			8.596	480
			8.856	500

Table A2. Experimental data for dysprosium

Temp. °C	P_{O_2} (atm.)	ln P_{O_2}	[Weight gain]^2 (mg.^{2})	Time (min.)
727	$10^{-0.3}$	-0.690	20.421	380
			21.288	400
			22.099	420
			22.924	440
	$10^{-1.342}$	-3.090	14.546	540
			14.992	560
			15.311	580
			15.665	600
			16.499	620
			16.875	640
	$10^{-3.3}$	-7.599	13.638	460
			13.950	480
			14.364	500
			14.730	520
			15.132	540
			15.649	560
			15.984	580
			16.443	600
			16.834	620
	$10^{-12.5}$	-28.787	22.752	380
			23.174	400
			23.512	420
			23.980	440
877	$10^{-0.3}$	-0.690	17.084	340
			18.045	360
			19.035	380
			20.061	400
			20.985	420
			22.061	440
			23.232	460
			24.245	480
			25.260	500
			26.163	520
			27.133	540
			28.164	560
	$10^{-1.342}$	-3.090	15.697	360
			16.900	380
			18.147	400
			19.307	420
			20.457	440

Table A2. (Continued)

Temp. °C	P_{O_2}(atm.)	ln P_{O_2}	[Weight gain]^2(mg.^{2})	Time (min.)
877	$10^{-3.3}$	-7.599	32.398	340
			32.695	360
			33.062	380
			33.396	400
			33.779	420
	$10^{-8.6}$	-19.805	28.569	420
			28.890	440
			29.116	460
			29.268	480
	$10^{-14.5}$	-33.393	41.088	400
			41.383	420
			41.615	440
			41.783	460
			42.146	480
			42.276	500
			42.510	520
1027	$10^{-0.3}$	-0.690	14.884	60
			15.792	70
			16.353	80
	$10^{-1.342}$	-3.090	15.952	80
			17.040	90
			17.867	100
	$10^{-3.3}$	-7.599	26.832	100
			27.164	110
			27.405	120
			27.657	130
	$10^{-5.6}$	-12.896	15.358	70
			15.437	80
			15.610	90
			15.634	100
			15.832	110
			15.960	120
			16.120	130
	$10^{-11.6}$	-26.715	32.775	110
			32.993	120
			33.131	130
			33.143	140
			33.166	150

Table A2. (Continued)

Temp. °C	P_{O_2} (atm.)	ln P_{O_2}	[Weight gain]^2 (mg.^{2})	Time (min.)
1027	$10^{-13.6}$	-31.321	23.872	120
			23.882	130
			24.088	140
			24.295	150
1177	$10^{-0.3}$	-0.690	20.412	40
			22.963	45
			24.433	50
	$10^{-1.342}$	-3.090	20.430	70
			24.049	80
			26.904	90
	$10^{-3.3}$	-7.599	23.164	40
			24.730	44
			25.522	48
	$10^{-9.3}$	-21.417	6.451	160
			7.123	180
			7.656	200
			8.236	220
			8.785	240
			9.388	260
	$10^{-11.3}$	-26.023	2.560	120
			2.913	140
			3.261	160
			3.591	180
			3.940	200
			4.272	220
			4.626	240
			4.959	260
1327	$10^{-0.3}$	-0.690	9.634	8
			10.510	10
			11.771	12
			13.003	14
			14.167	16
			15.272	18
	$10^{-1.342}$	-3.090	9.935	12
			10.903	14
			11.833	16
			12.666	18

Table A2. (Continued)

Temp. °C	P_{O_2} (atm.)	ln P_{O_2}	[Weight gain]^2 (mg.^{2})	Time (min.)
1327	$10^{-3.3}$	-7.599	18.003	26
			18.835	28
			19.695	30
			20.720	32
			21.650	34
			22.486	36
			23.328	38
	$10^{-7.3}$	-16.811	16.818	28
			17.189	30
			17.901	32
			18.464	34
			18.992	36
			19.527	38
			20.070	40
			20.557	42
			21.114	44
	$10^{-9.3}$	-21.417	13.329	28
			13.838	30
			14.318	32
			14.853	34
			15.311	36
			15.792	38
			16.257	40